Documentation of the ARIES/GEOS Dynamical Core Version 2

Max J. Suarez
Climate and Radiation Branch

and

Lawrence L. Takacs
Data Assimilation Office

Laboratory for Atmospheres
Goddard Space Flight Center
Greenbelt, Maryland 20771

August 12, 1994

Abstract

A detailed description of the numerical formulation of Version 2 of the ARIES/GEOS "dynamical core" is presented. This code is a nearly "plug-compatible" dynamics for use in atmospheric general circulation models (GCMs). It is a finite difference model on a staggered latitude-longitude C-grid. It uses second-order differences for all terms except the advection of vorticity by the rotational part of the flow, which is done at fourth-order accuracy. This dynamical core is currently being used in the climate (ARIES) and data assimilation (GEOS) GCMs at Goddard.

Contents

List of Figures

1 Introduction

The need to use modular coding techniques in atmospheric general circulation models (GCMs) has been recognized for some time. The two main benefits of this approach are that it makes codes much easier to maintain and modify, particularly when the work must be done by several people, and that it makes it easier to exchange and compare codes. Modular coding practices are thus being used to some extent by most atmospheric modelers; but most of the effort has gone into developing modular codes for the physical parameterizations, such as radiation and cumulus convection. Kalnay et al (1989) proposed a set of rules for coding physical parameterizations aimed at facilitating the exchange of codes. If these "plug-compatible" rules are followed in coding both the GCMs and the parameterizations, codes can be "unplugged" from one model and "plugged" into another with little effort.

In this report we introduce the notion of a "dynamical core," which attempts to extend the ideas of plug-compatible parameterizations to the coding of the dynamics. Since the manner in which the equations of motion are discretized affects so fundamentally the organization of both the code and the data in a GCM, it is not practical to make the dynamics codes truly plug compatible. They can, however, be made sufficiently modular that—once the GCM's data structure is modified to accommodate them—the computational routines can be easily ported.

The dynamical core we will be describing consists of a complete set of subroutines that compute the time tendencies of winds, temperatures, surface pressure, and an arbitrary number of tracers. The core is invoked by calling a single subroutine, and all data is passed to the core through that subroutine's argument list. Inputs to the core include: the dimensions of the grid, an array defining the vertical distribution of the layers, some physical parameters, the state variables at two time levels, the time step, and the time tendencies of each state variable due to other processes. The core updates the time tedencies to include the effects of the dynamics. It does not update the state variables, or perform any temporal or spatial damping that may be needed to control non-linear computational instability.

Ideally one would want the core to be independent of the time differencing, but this is not possible except for the simplest explicit differencing. By passing the time step, two time levels of state variables, and tendencies due to other processes, the core can compute tendencies for other time differencing methods, such as the semi-implicit scheme commonly used in spectral models. The version we describe here is for explicit time differencing only, but it can produce "economical explicit" tendencies (Brown and Campana 1978) for use with a leap-frog scheme.

All state variables and tendencies in the argument list are on the core's horizontal and vertical grids—in our case, an unstaggered or Lorenz grid in standard sigma coordinates in the vertical and an Arakawa C grid in the horizontal. Although the type of discretization is determined by the dynamical core—and the GCM's data structure must conform to it—

other things, such as the resolution or the placement of the layers in the vertical, need not be. In our dynamical core, these are controlled through the argument list and are thus completely arbitrary. (The resolution can even be altered from one call to another within a single program.) Thus, the core can be adapted to many applications by simply altering the call, rather than modifying the source and rebuilding the binaries. This should simplify the use of the core for those not interested in tinkering with the source code.

The differencing used in the ARIES/GEOS core follows closely that which has been in use in the UCLA GCM since around 1980. Both the ARIES/GEOS core and the UCLA model are based on a C grid, they use the same spherical grid, they both use Arakawa and Suarez (1983) vertical differencing, and they use similar forms of the momentum equation. There are, however, a number of important differences. The UCLA model, for example, uses a modified sigma coordinate, while the ARIES/GEOS core uses standard sigma. Rather than detailing these differences, we will present a complete description of the ARIES/GEOS core.

This documentation is for Version 2 of the core. Version 1 is very similar, differing primarily in that it uses a second order scheme for advection in the momentum equation. It has been used for a number of applications at Goddard, including the re-analysis currently underway at the Data Assimilation Office.

The presentation follows the general form and notation of Arakawa and Lamb (1977), repeating their discussion of the continuous equations in sections 2 and 3, then presenting the vertical differencing in section 4 and the horizontal differencing in section 5. The new fourth-order scheme for advection of vorticity is presented in section 5. Section 6 describes the polar filters, and section 7 the interaction of the dynamical core with the time differencing. Section 8 describes the FORTRAN interface and gives a brief overview of the structure of the code. Section 9 presents results from several test integrations, comparing the current version with a spectral dynamics under idealized forcing and with Version 1 using a full GCM.

2 Continuous Equations

We use a σ coordinate defined by

$$\sigma = \frac{p - p_T}{\pi}, \tag{1}$$

where p is the pressure, $\pi \equiv p_s - p_T$, p_s is the surface pressure, and p_T is a constant prescribed pressure at the top of the model atmosphere. With $p_T = 0$ this coordinate reduces to the conventional σ coordinate proposed by Phillips (1957). The code is written in this more general σ coordinate for backward compatibility with earlier versions of our GCMs; in the current versions, however, we take $p_T = 0$.

With this vertical coordinate, the continuity equation becomes

$$\frac{\partial \pi}{\partial t} = -\nabla_\sigma \cdot (\pi \mathbf{v}) - \frac{\partial(\pi \dot{\sigma})}{\partial \sigma}, \tag{2}$$

where $\mathbf{v}$ is the horizontal velocity vector. Integrating (2) and assuming $\dot{\sigma} = 0$ at $p = 0$ and $p = p_T$, we obtain the forms used in the model:

$$\frac{\partial \pi}{\partial t} = -\int_0^1 \nabla_\sigma \cdot (\pi \mathbf{v})\, d\sigma \tag{3}$$

and

$$(\pi \dot{\sigma}) = -\sigma \frac{\partial \pi}{\partial t} - \int_0^\sigma \nabla_\sigma \cdot (\pi \mathbf{v})\, d\sigma. \tag{4}$$

The equation of state for an ideal gas is $\alpha = RT/p$, where α is the specific density, T is the temperature, and R is the gas constant. The following alternative forms will be used below

$$\alpha = R\theta \frac{P}{p} = c_p \theta \frac{\partial P}{\partial p} = \frac{c_p \theta}{\pi} \left(\frac{\partial P}{\partial \sigma} \right)_\pi = \frac{c_p \theta}{\sigma} \left(\frac{\partial P}{\partial \pi} \right)_\sigma, \tag{5}$$

where $\theta \equiv T/P$ is the potential temperature, $P \equiv (p/p_0)^\kappa$, $\kappa = R/c_p$, c_p is the specific heat at constant pressure, and p_0 is a reference pressure. In obtaining the forms in (5) we have used $\frac{\partial P}{\partial p} = \kappa \frac{P}{p}$ and the relation

$$\left(\frac{dP}{d\sigma} \right)_\pi = \frac{\pi}{\sigma} \left(\frac{dP}{d\pi} \right)_\sigma. \tag{6}$$

For the time being we are ignoring virtual effects.

The hydrostatic equation is

$$\frac{\partial \Phi}{\partial p} = -\alpha,$$

where Φ is the geopotential. Using (1), (5), and (6), this can be written:

$$\frac{\partial \Phi}{\partial \sigma} = -\pi \alpha = -c_p \theta \frac{\pi}{\sigma} \left(\frac{dP}{d\pi} \right)_\sigma = -c_p \theta \left(\frac{dP}{d\sigma} \right)_\pi. \tag{7}$$

From (7) we obtain

$$\frac{\partial \Phi}{\partial P} = -c_p \theta, \tag{8}$$

which is the form used by Arakawa and Suarez (1983) for vertical discretization.

The thermodynamic equation is written in flux form to facilitate the derivation of a θ-conserving differencing scheme:

$$\frac{\partial(\pi \theta)}{\partial t} = -\nabla_\sigma \cdot (\pi \mathbf{v} \theta) - \frac{\partial(\pi \dot{\sigma} \theta)}{\partial \sigma} + \frac{\pi Q}{c_p P}, \tag{9}$$

where $\mathcal{Q}$ is the diabatic heating per unit mass.

In addition to the equations of motion, the core computes tendencies for an arbitrary number of atmospheric constituents, such as water vapor and ozone. These are also written in flux form:

$$\frac{\partial(\pi q^{(k)})}{\partial t} = -\nabla_\sigma \cdot (\pi \mathbf{v} q^{(k)}) - \frac{\partial(\pi \dot{\sigma} q^{(k)})}{\partial \sigma} + \pi \mathcal{S}^{(k)}, \tag{10}$$

where $q^{(k)}$ is the specific mass of the kth constituent, and $\mathcal{S}^{(k)}$ is its source per unit mass of air.

The momentum equation is written in "vector-invariant" form, as in Sadourney (1975) and Arakawa and Lamb (1981), to facilitate the derivation of an energy- and enstrophy-conserving differencing scheme:

$$\begin{aligned}
\frac{\partial \mathbf{v}}{\partial t} &= -(f+\zeta)\,\mathbf{k}\times\mathbf{v} - \dot{\sigma}\frac{\partial \mathbf{v}}{\partial \sigma} - \nabla_\sigma(\Phi + K) - c_p\theta\,\nabla_\sigma P - \frac{g}{\pi}\frac{\partial \mathcal{T}}{\partial \sigma}, &(11)\\
&= -\eta\,\mathbf{k}\times(\pi\mathbf{v}) - \dot{\sigma}\frac{\partial \mathbf{v}}{\partial \sigma} - \nabla_\sigma(\Phi + K) - c_p\theta\left(\frac{dP}{d\pi}\right)_\sigma \nabla\pi - \frac{g}{\pi}\frac{\partial \mathcal{T}}{\partial \sigma}, &(12)
\end{aligned}$$

where f is the Coriolis parameter, $\mathbf{k}$ is the unit vector in the vertical,

$$\zeta \equiv \nabla_\sigma \times \mathbf{v}$$

is the vertical component of the vorticity along σ surfaces,

$$\eta = \frac{(f+\zeta)}{\pi}$$

is an "external" potential vorticity,

$$K \equiv \frac{1}{2}(\mathbf{v}\cdot\mathbf{v})$$

is the kinetic energy per unit mass, g is the acceleration of gravity, and $\mathcal{T}$ is the horizontal frictional stress vector.

3 Conservation Properties

Integrating (2) over the entire atmosphere we obtain a statement of conservation of total atmospheric mass,

$$\frac{\partial}{\partial t}\int_S \pi\, ds = 0,$$

where S represents the surface of the sphere. Similarly integrating (9) and (10), we obtain equations for the global mass-weighted integrals of θ and q:

$$\frac{\partial}{\partial t}\int_S\int_0^1 (\pi\theta)\, d\sigma ds = \int_S\int_0^1 \left(\frac{\pi\mathcal{Q}}{c_p P}\right) d\sigma ds$$

and

$$\frac{\partial}{\partial t}\int_S\int_0^1 (\pi q^{(k)})\, d\sigma ds = \int_S\int_0^1 (\pi \mathcal{S}_{q^{(k)}}) d\sigma ds.$$

To discuss conservation of total energy, we first write an equation for the temperature. Multiplying (9) by $c_p P$ we obtain:

$$\begin{aligned}\frac{\partial(\pi c_p T)}{\partial t} &= -\nabla_\sigma \cdot (\pi \mathbf{v} c_p T) - \frac{\partial(\pi\dot{\sigma} c_p T)}{\partial\sigma} \\ &+ \pi c_p \theta \left(\frac{\partial P}{\partial t} + \mathbf{v}\cdot\nabla_\sigma P + \dot{\sigma}\frac{\partial P}{\partial \sigma}\right) + \pi \mathcal{Q}. \end{aligned} \tag{13}$$

The first two terms on the right-hand side of (13) vanish when integrated over the entire domain. The first term on the second line represents the conversion to kinetic energy. Using (6), this term can be written as:

$$\frac{\pi c_p \theta}{\sigma}\left(\frac{dP}{d\pi}\right)_\sigma \left[\sigma\left(\frac{\partial \pi}{\partial t} + \mathbf{v}\cdot\nabla\pi\right) + \pi\dot{\sigma}\right]. \tag{14}$$

The thermodynamic equation can then be written in the more conventional form:

$$\frac{\partial(\pi c_p T)}{\partial t} = -\nabla_\sigma \cdot (\pi \mathbf{v} c_p T) - \frac{\partial(\pi\dot{\sigma} c_p T)}{\partial\sigma} + (\pi\omega\alpha) + \pi\mathcal{Q}, \tag{15}$$

where ω is the vertical p velocity:

$$\omega \equiv \dot{p} = \pi\dot{\sigma} + \sigma\left(\frac{\partial\pi}{\partial t} + \mathbf{v}\cdot\nabla\pi\right), \tag{16}$$

and α is given by (5).

Next we obtain the kinetic energy equation by dotting $(\pi\mathbf{v})$ with (12). The first term on the right-hand side of (12) is an "inertial force," which does no work since it acts normal to the motion. The remaining terms give:

$$\begin{aligned}\frac{\partial(\pi K)}{\partial t} &= -\nabla_\sigma\cdot(\pi\mathbf{v}K) - \frac{\partial(\pi\dot{\sigma}K)}{\partial\sigma} + K\left(\frac{\partial\pi}{\partial t} + \nabla_\sigma\cdot(\pi\mathbf{v}) + \frac{\partial(\pi\dot{\sigma})}{\partial\sigma}\right) \\ &- (\pi\mathbf{v})\cdot\left(\nabla_\sigma\Phi + c_p\theta\left(\frac{dP}{d\pi}\right)_\sigma \nabla\pi\right) - g\mathbf{v}\cdot\frac{\partial\mathcal{T}}{\partial\sigma}.\end{aligned} \tag{17}$$

The last term on the right-hand side of the first line vanishes from conservation of mass (17). Terms on the second line represent the work done by the pressure-gradient force—the conversion from potential energy. We next consider the first of these, $-(\pi\mathbf{v}\cdot\nabla_\sigma\Phi)$:

$$\begin{aligned}-(\pi\mathbf{v}\cdot\nabla_\sigma\Phi) &= -\nabla_\sigma\cdot(\pi\mathbf{v}\Phi) - \Phi\left(\frac{\partial\pi}{\partial t} + \frac{\partial(\pi\dot{\sigma})}{\partial\sigma}\right) \\ &= -\nabla_\sigma\cdot(\pi\mathbf{v}\Phi) - \frac{\partial(\pi\dot{\sigma}\Phi)}{\partial\sigma} - \Phi\frac{\partial\pi}{\partial t} + \pi\dot{\sigma}\frac{\partial\Phi}{\partial\sigma}\end{aligned}$$

$$
\begin{aligned}
&= -\nabla_\sigma \cdot (\pi \mathbf{v} \Phi) - \frac{\partial(\pi \dot{\sigma} \Phi)}{\partial \sigma} - \frac{\partial(\sigma \Phi)}{\partial \sigma}\frac{\partial \pi}{\partial t} + \frac{\partial \Phi}{\partial \sigma}\left(\pi \dot{\sigma} + \sigma \frac{\partial \pi}{\partial t}\right) \\
&= -\nabla_\sigma \cdot (\pi \mathbf{v} \Phi) - \frac{\partial(\pi \dot{\sigma} \Phi)}{\partial \sigma} - \frac{\partial(\sigma \Phi)}{\partial \sigma}\frac{\partial \pi}{\partial t} - \frac{\pi c_p \theta}{\sigma}\left(\frac{\partial P}{\partial \pi}\right)_\sigma \left(\pi \dot{\sigma} + \sigma \frac{\partial \pi}{\partial t}\right), \qquad (18)
\end{aligned}
$$

where we have used (2), (7), and the identity

$$
\Phi = \frac{\partial(\sigma \Phi)}{\partial \sigma} - \sigma \frac{\partial \Phi}{\partial \sigma}. \qquad (19)
$$

The kinetic energy equation (13) can now be rewritten as

$$
\begin{aligned}
\frac{\partial(\pi K)}{\partial t} = & -\nabla_\sigma \cdot (\pi \mathbf{v} K) - \frac{\partial(\pi \dot{\sigma} K)}{\partial \sigma} - \nabla_\sigma \cdot (\pi \mathbf{v} \Phi) - \frac{\partial(\pi \dot{\sigma} \Phi)}{\partial \sigma} \\
& - \frac{\partial(\sigma \Phi)}{\partial \sigma}\frac{\partial \pi}{\partial t} - \frac{\pi c_p \theta}{\sigma}\left(\frac{\partial P}{\partial \pi}\right)_\sigma \left[\pi \dot{\sigma} + \sigma \left(\frac{\partial \pi}{\partial t} + \mathbf{v} \cdot \nabla \pi\right)\right] - g\mathbf{v} \cdot \frac{\partial \mathcal{T}}{\partial \sigma}. \qquad (20)
\end{aligned}
$$

Finally, using (16) and (5), we obtain a kinetic energy equation in which the conversion term is written in the same form as in (15).

$$
\begin{aligned}
\frac{\partial(\pi K)}{\partial t} = & -\nabla_\sigma \cdot (\pi \mathbf{v} K) - \frac{\partial(\pi \dot{\sigma} K)}{\partial \sigma} - \nabla_\sigma \cdot (\pi \mathbf{v} \Phi) - \frac{\partial(\pi \dot{\sigma} \Phi)}{\partial \sigma} \\
& - \frac{\partial(\sigma \Phi)}{\partial \sigma}\frac{\partial \pi}{\partial t} - (\pi \omega \alpha) - g\mathbf{v} \cdot \frac{\partial \mathcal{T}}{\partial \sigma}. \qquad (21)
\end{aligned}
$$

Summing (15) and (21) and integrating over the entire domain, we obtain an equation for the rate of change of the total energy of the atmosphere:

$$
\frac{\partial}{\partial t}\int_S \int_0^1 (c_p T + K + \Phi_s)\frac{\pi \, d\sigma}{g} ds = \int_S \int_0^1 \left(\mathcal{Q} - \frac{g}{\pi}\mathbf{v} \cdot \frac{\partial \mathcal{T}}{\partial \sigma}\right)\frac{\pi \, d\sigma}{g} ds, \qquad (22)
$$

where Φ_s is the surface geopotential.

3.1 The Vertically Integrated Pressure Gradient Force

The vertical integral of the pressure gradient force is irrotational in the absence of spatial variations of the surface geopotential. This must be so if the system is to conserve angular momentum in the absence of "mountain torques" or other horizontal stresses. This property is easily verified by taking the curl of the vertically integrated pressure gradient force or, more instructively, by writing it in terms of the gradient of the surface geopotential:

$$
\begin{aligned}
\int_{p_T}^{p_s} \nabla_p \Phi \, dp &= \nabla \left[\int_{p_T}^{p_s} \Phi \, dp\right] - \Phi_s \nabla p_s, \\
&= \nabla \left[\int_{p_T}^{p_s} (\Phi - \Phi_s) \, dp\right] + (p_s - p_T) \nabla \Phi_s, \\
&= \nabla \left[\int_0^1 \pi (\Phi - \Phi_s) \, d\sigma\right] + \pi \nabla \Phi_s. \qquad (23)
\end{aligned}
$$

In the last two forms, the curl of the first term is zero and the second term vanishes if Φ_s is constant.

To satisfy this property in the discrete model, we will need to obtain this form starting from the pressure gradient force written in terms of gradients along σ surfaces.

$$\begin{aligned}
\int_0^1 \pi \nabla_p \Phi \, d\sigma &= \int_0^1 \pi \left[\nabla_\sigma \Phi + c_p \theta \left(\frac{dP}{d\pi} \right)_\sigma \nabla \pi \right] d\sigma, \\
&= \nabla \left[\int_0^1 (\pi \Phi) \, d\sigma \right] - \nabla \pi \int_0^1 \left[\Phi + \sigma \frac{\partial \Phi}{\partial \sigma} \right] d\sigma, \\
&= \nabla \left[\int_0^1 (\pi \Phi) \, d\sigma \right] - \Phi_s \nabla \pi, \\
&= \nabla \left[\int_0^1 \pi (\Phi - \Phi_s) \, d\sigma \right] + \pi \nabla \Phi_s,
\end{aligned} \tag{24}$$

where we have used (7) and (19).

4 Vertical Differencing

4.1 The Vertical Grid

We use a Lorenz grid in the vertical, with both winds and temperatures defined at the same levels. The atmosphere between $\sigma = 0$ and $\sigma = 1$ is divided into LM layers by $\mathrm{LM} - 1$ surfaces of specified constant σ_l, $l = 2, \mathrm{LM}$, so that $\sigma_1 = 0$ corresponds to the top of the model atmosphere, and $\sigma_{\mathrm{LM}+1} = 1$ corresponds to the lower boundary. At the LM layers we define the velocity, $\mathbf{v}_l$, the potential temperature, θ_l, and the specific masses of all trace constituents, $q_l^{(k)}$. The vertical σ velocity, $\dot{\sigma}_l$, is defined at the interfaces between the layers and at the top and bottom surface. This arrangement of the variables is shown schematically in figure 1.

Note that both layers and interface levels are numbered from top to bottom and that, to maintain as close a correspondence with the code as possible, both are indexed by integers, rather than using the more common convention of assigning the interfaces half-integer values. Level σ_l thus corresponds to the top of layer l. Where there might be some confusion as to whether a quantity is defined at the layers or at the interfaces, we will mark the interface quantities with a hat (viz., $\hat{P}$). Vertical differences will thus be written as

$$(\delta \hat{a})_l = \hat{a}_{l+1} - \hat{a}_l$$

at the layers, and

$$\widehat{(\delta a)}_l = a_l - a_{l-1}$$

at the interfaces.

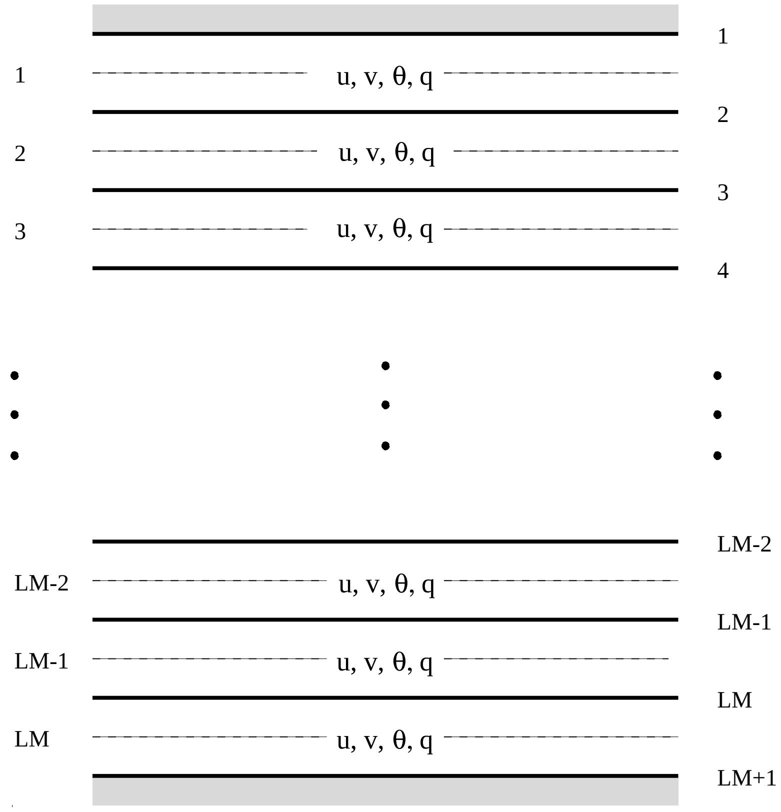

Figure 1: The vertical grid

4.2 The Discrete Equations

Using (1), we define the pressures at the top, bottom, and interface levels as: [1]

$$p_l = p_T + \pi\sigma_l, \quad \text{for } l = 1, \mathrm{LM}+1. \tag{\textbf{25}}$$

The values of the Exner function at the interfaces are obtained directly from (25):

$$\hat{P}_l = \left(\frac{p_l}{p_0}\right)^{\kappa}, \quad \text{for } l = 1, \mathrm{LM}+1, \tag{\textbf{26}}$$

[1]The forms of the equations used in the code will be denoted by boldface numbers.

which can be written

$$\hat{P}_l = \pi^\kappa \left(\frac{\sigma_l}{p_0}\right)^\kappa \equiv \pi^\kappa \hat{\mathcal{P}}_l \tag{26}$$

for $p_T = 0$. The latter form is much more economical to use since the first factor on the right-hand side is independent of l and the second factor, $\hat{\mathcal{P}}_l$, depends only on σ. The code takes advantage of such economies when $p_T = 0$ and uses the general form only when $p_T \neq 0$. We will thus write the $p_T = 0$ forms when appropriate.

Layer temperatures T_l are defined from the potential temperatures as $T_l = \theta_l P_l$, where P_l, the Exner function at the layers, is given by

$$P_l = \frac{1}{1+\kappa}\left[\frac{\delta(p\hat{P})}{\delta p}\right]_l, \quad \text{for } l = 1, \mathrm{LM}. \tag{27}$$

This is the form proposed by Phillips (1974). For $p_T = 0$ this becomes

$$P_l = \frac{\pi^\kappa}{p_0^\kappa(1+\kappa)}\left[\frac{\delta\sigma^{\kappa+1}}{\delta\sigma}\right]_l \equiv \pi^\kappa \mathcal{P}_l, \tag{27a}$$

where again $\mathcal{P}_l$ depends only on σ.

The vertical finite differencing of the thermodynamic and hydrostatic equations and of the pressure gradient force follows Arakawa and Suarez (1983). In their scheme, the potential temperature "interpolated" to the interfaces is

$$\hat{\theta}_{l+1} = \frac{(P_{l+1} - \hat{P}_{l+1})\theta_{l+1} + (\hat{P}_{l+1} - P_l)\theta_l}{P_{l+1} - P_l}, \quad \text{for } l = 1, \mathrm{LM}-1. \tag{28}$$

As we show below, to conserve energy this form has to be used in the hydrostatic equation for the thickness between layers and in the vertical advection term in the thermodynamic equation. When $p_T = 0$, (28) becomes:

$$\hat{\theta}_{l+1} = \frac{\mathcal{P}_{l+1} - \hat{\mathcal{P}}_{l+1}}{\mathcal{P}_{l+1} - \mathcal{P}_l}\theta_{l+1} + \frac{\hat{\mathcal{P}}_{l+1} - \mathcal{P}_l}{\mathcal{P}_{l+1} - \mathcal{P}_l}\theta_l, \tag{29}$$

so that the interpolation depends only on σ, not pressure.

The hydrostatic equation is

$$\begin{aligned}
\Phi_{\mathrm{LM}} &= \Phi_s + c_p\theta_{\mathrm{LM}}(\hat{P}_{\mathrm{LM}+1} - P_{\mathrm{LM}}), & \textbf{(30)}\\
\Phi_l &= \Phi_{l+1} + c_p\hat{\theta}_{l+1}(P_{l+1} - P_l), & \\
&= \Phi_{l+1} + c_p[(P_{l+1} - \hat{P}_{l+1})\theta_{l+1} + (\hat{P}_{l+1} - P_l)\theta_l], \quad \text{for } l = 1, \mathrm{LM}-1. & \textbf{(31)}
\end{aligned}$$

For $p_T = 0$ we write this as:

$$\begin{aligned}
\Phi_{\mathrm{LM}} &= \Phi_s + c_p\theta_{\mathrm{LM}}\pi^\kappa(\hat{\mathcal{P}}_{\mathrm{LM}+1} - \mathcal{P}_{\mathrm{LM}}), & \textbf{(30a)}\\
\Phi_l &= \Phi_{l+1} + c_p\pi^\kappa[(\mathcal{P}_{l+1} - \hat{\mathcal{P}}_{l+1})\theta_{l+1} + (\hat{\mathcal{P}}_{l+1} - \mathcal{P}_l)\theta_l]. & \textbf{(31a)}
\end{aligned}$$

The continuity equation is

$$\frac{\partial \pi}{\partial t} = -\nabla \cdot (\pi \mathbf{v}_l) - \left(\frac{\delta(\pi \dot{\sigma})}{\delta \sigma} \right)_l, \tag{32}$$

The equation for the tendency of π is obtained by summing (32):

$$\frac{\partial \pi}{\partial t} = -\sum_{\ell=1}^{\mathrm{LM}} \nabla \cdot (\pi \mathbf{v}_\ell)\ (\delta\sigma)_\ell, \tag{33}$$

and the vertical σ velocity at the interfaces is given by

$$(\pi\dot{\sigma})_{l+1} = -\sigma_{l+1}\frac{\partial \pi}{\partial t} - \sum_{\ell=1}^{l} \nabla \cdot (\pi \mathbf{v}_\ell)\ (\delta\sigma)_\ell, \qquad \text{for } l = 1, \mathrm{LM}-1. \tag{34}$$

The thermodynamic equation is

$$\frac{\partial(\pi\theta_l)}{\partial t} = -\nabla \cdot (\pi \mathbf{v}_l \theta_l) - \left(\frac{\delta(\pi\dot{\sigma}\,\hat{\theta})}{\delta\sigma} \right)_l + \frac{\pi\, Q_l}{c_p P_l}, \qquad \text{for } l = 1, \mathrm{LM}, \tag{35}$$

where $\hat{\theta}_l$ is given by (28) and P_l by (27). We note that using (28) as the interpolation of θ for vertical advection gives up conservation of θ^2 or some other function of θ. This is the price Arakawa-Suarez pays to use a local hydrostatic equation. The scheme of Arakawa (1972) satisfies all conservation properties of Arakawa-Suarez *plus* conservation of a function of θ, but it uses a non-local hydrostatic equation, in which one of the geopotentials depends on a weighted sum of all the temperatures in the column.

For advection of the trace constituents, we are currently using the square-conserving form:

$$\frac{\partial(\pi q_l^{(k)})}{\partial t} = -\nabla \cdot (\pi \mathbf{v}_l q_l^{(k)}) - \left(\frac{\delta(\pi\dot{\sigma}\,\hat{q}^{(k)})}{\delta\sigma} \right)_l + \pi \mathcal{S}_l^{(k)}, \qquad \text{for } l = 1, \mathrm{LM}, \tag{36}$$

where

$$\hat{q}_{l+1}^{(k)} = \frac{1}{2}\left(q_{l+1}^{(k)} + q_l^{(k)} \right), \qquad \text{for } l = 1, \mathrm{LM}-1. \tag{37}$$

The form of the momentum equation is:

$$\begin{aligned} \frac{\partial \mathbf{v}_l}{\partial t} \quad &= \quad -\eta_l\ \mathbf{k} \times (\pi \mathbf{v}_l) - \frac{1}{2}\frac{1}{(\delta\sigma)_l}\left[\dot{\sigma}_l(\mathbf{v}_l - \mathbf{v}_{l-1}) + \dot{\sigma}_{l+1}(\mathbf{v}_{l+1} - \mathbf{v}_l)\right] \\ &\quad - \nabla(\Phi + K)_l - c_p\theta_l \left(\frac{dP}{d\pi}\right)_l \nabla\pi - \frac{g}{\pi}\left(\frac{\delta \mathcal{T}}{\delta\sigma}\right)_l, \qquad \text{for } l = 1, \mathrm{LM}, \end{aligned} \tag{38}$$

where

$$\left(\frac{dP}{d\pi}\right)_l = \frac{\sigma_{l+1}(\hat{P}_{l+1} - P_l) + \sigma_l(P_l - \hat{P}_l)}{\pi(\delta\sigma)_l}, \qquad \text{for } l = 1, \text{LM}. \tag{39}$$

With $p_T = 0$, (39) becomes:

$$\left(\frac{dP}{d\pi}\right)_l = \frac{\pi^\kappa}{\pi} \frac{\sigma_{l+1}(\hat{\mathcal{P}}_{l+1} - \mathcal{P}_l) + \sigma_l(\mathcal{P}_l - \hat{\mathcal{P}}_l)}{(\delta\sigma)_l}, \tag{39a}$$

where, again, the second factor depends only on σ.

4.3 Energy Conservation and the Discrete ω

The derivation and justification of the vertical differencing scheme presented above is given in Arakawa and Suarez (1983). Here we will merely show that these differential-difference equations are energy conserving. We will also obtain a discrete form of ω from the energy conversion term.

We start, as in section 2, by writing the thermodynamic equation in terms of the temperature at the layers, $T_l = P_l\theta_l$. Multiplying (35) by $c_p P_l$ we have:

$$\begin{aligned}
\frac{\partial(\pi c_p T_l)}{\partial t} &= -\nabla\cdot(\pi \mathbf{v}_l c_p T_l) - P_l\left(\frac{\delta(\pi\dot{\sigma}c_p\hat{\theta})}{\delta\sigma}\right)_l + c_p\theta_l\pi\left[\frac{\partial P_l}{\partial t} + \mathbf{v}_l\cdot\nabla P_l\right] + \pi\mathcal{Q}_l, \\
&= -\nabla\cdot(\pi \mathbf{v}_l c_p T_l) - \left(\frac{\delta(\pi\dot{\sigma}c_p\hat{T})}{\delta\sigma}\right)_l \\
&\qquad \boxed{+\frac{c_p}{(\delta\sigma)_l}\left[(\pi\dot{\sigma})_{l+1}(\hat{T}_{l+1} - P_l\hat{\theta}_{l+1}) - (\pi\dot{\sigma})_l(\hat{T}_l - P_l\hat{\theta}_l)\right]} \\
&\qquad \boxed{+ c_p\theta_l\pi\left(\frac{dP}{d\pi}\right)_l\left[\frac{\partial\pi}{\partial t} + \mathbf{v}_l\cdot\nabla\pi\right],} + \pi\mathcal{Q}_l \qquad \text{for } l = 1, \text{LM}.
\end{aligned} \tag{40}$$

Here the quantity $\hat{T}$ has been introduced to put the equation in flux form; this allows us to separate the energy conversion term. Comparing (40) with (15), we see that boxed terms of (40) correspond to $(\pi\omega\alpha)_l$.

To form the kinetic energy equation we multiply (38) by $\pi\mathbf{v}_l$:

$$\begin{aligned}
\frac{\partial \pi K_l}{\partial t} &= -\nabla\cdot(\pi\mathbf{v}_l K_l) + K_l\left(\frac{\partial\pi}{\partial t} + \nabla\cdot(\pi\mathbf{v}_l) + \left(\frac{\delta(\pi\dot{\sigma})}{\delta\sigma}\right)_l\right) \\
&\quad - \frac{1}{2}\frac{1}{(\delta\sigma)_l}\left((\pi\dot{\sigma})_{l+1}\mathbf{v}_{l+1}\cdot\mathbf{v}_l - (\pi\dot{\sigma})_l\mathbf{v}_l\cdot\mathbf{v}_{l-1}\right)
\end{aligned}$$

$$
\begin{aligned}
& - \nabla \cdot (\pi \mathbf{v}_l \Phi_l) + \Phi_l \nabla \cdot (\pi \mathbf{v}_l) - c_p \theta_l \pi \left(\frac{dP}{d\pi}\right)_l \mathbf{v}_l \cdot \nabla \pi - g \mathbf{v}_l \cdot \left(\frac{\delta \mathcal{T}}{\delta \sigma}\right)_l , \\
= \; & -\nabla \cdot (\pi \mathbf{v}_l K_l) - \frac{1}{2} \frac{1}{(\delta \sigma)_l} ((\pi \dot{\sigma})_{l+1} \mathbf{v}_{l+1} \cdot \mathbf{v}_l - (\pi \dot{\sigma})_l \mathbf{v}_l \cdot \mathbf{v}_{l-1}) \\
& - \nabla \cdot (\pi \mathbf{v}_l \Phi_l) - \Phi_l \left(\frac{\partial \pi}{\partial t} + \left(\frac{\delta (\pi \dot{\sigma})}{\delta \sigma} \right)_l \right) - c_p \theta_l \pi \left(\frac{dP}{d\pi}\right)_l \mathbf{v}_l \cdot \nabla \pi - g \mathbf{v}_l \cdot \left(\frac{\delta \mathcal{T}}{\delta \sigma}\right)_l , \\
= \; & -\nabla \cdot (\pi \mathbf{v}_l K_l) - \frac{1}{2} \frac{1}{(\delta \sigma)_l} ((\pi \dot{\sigma})_{l+1} \mathbf{v}_{l+1} \cdot \mathbf{v}_l - (\pi \dot{\sigma})_l \mathbf{v}_l \cdot \mathbf{v}_{l-1}) \\
& - \nabla \cdot (\pi \mathbf{v}_l \Phi_l) - \left(\frac{\delta (\hat{\Phi} \pi \dot{\sigma})}{\delta \sigma} \right)_l - \left(\frac{\delta (\Phi \sigma)}{\delta \sigma} \right)_l \frac{\partial \pi}{\partial t} - g \mathbf{v}_l \cdot \left(\frac{\delta \mathcal{T}}{\delta \sigma}\right)_l \\
& \boxed{ + \frac{(\pi \dot{\sigma})_{l+1} (\hat{\Phi}_{l+1} - \Phi_l) + (\pi \dot{\sigma})_l (\Phi_l - \hat{\Phi}_l)}{(\delta \sigma)_l} } \\
& \boxed{ + \frac{\sigma_{l+1} (\hat{\Phi}_{l+1} - \Phi_l) + \sigma_l (\Phi_l - \hat{\Phi}_l)}{(\delta \sigma)_l} \frac{\partial \pi}{\partial t} - c_p \theta_l \pi \left(\frac{dP}{d\pi}\right)_l \mathbf{v}_l \cdot \nabla \pi , } \quad \text{for } l = 1, \mathrm{LM}, \qquad (41)
\end{aligned}
$$

where we have used the continuity equation (32) and the relations:

$$
\Phi_l = \left(\frac{\delta (\Phi \sigma)}{\delta \sigma} \right)_l - \frac{\sigma_{l+1} (\hat{\Phi}_{l+1} - \Phi_l) + \sigma_l (\Phi_l - \hat{\Phi}_l)}{(\delta \sigma)_l}, \qquad (42)
$$

which is a finite differenced analog of (19), and

$$
\Phi_l \left(\frac{\delta (\pi \dot{\sigma})}{\delta \sigma} \right)_l = \left(\frac{\delta (\hat{\Phi} \pi \dot{\sigma})}{\delta \sigma} \right)_l - \frac{(\pi \dot{\sigma})_{l+1} (\hat{\Phi}_{l+1} - \Phi_l) + (\pi \dot{\sigma})_l (\Phi_l - \hat{\Phi}_l)}{(\delta \sigma)_l}. \qquad (43)
$$

Comparing (41) with (21), we see that the boxed terms in (41) correspond to the conversion term, $-(\pi \omega \alpha)_l$. Energy conservation requires that the forms of $(\pi \omega \alpha)_l$ in (40) and (41) be identical. Comparing quantities in the first box in each equation and noting that $\dot{\sigma}_1 = \dot{\sigma}_{\mathrm{LM}+1} = 0$, we see that we must require that

$$
\begin{aligned}
c_p (\hat{T}_{l+1} - P_l \hat{\theta}_{l+1}) &= \Phi_l - \hat{\Phi}_{l+1}, && \text{for } l = 1, \mathrm{LM}-1, && (44a) \\
c_p (\hat{T}_l - P_l \hat{\theta}_l) &= \Phi_l - \hat{\Phi}_l, && \text{for } l = 2, \mathrm{LM}. && (44b)
\end{aligned}
$$

Similarly, considering the second boxes in each equation we must require that

$$
\frac{\sigma_{l+1} (\hat{\Phi}_{l+1} - \Phi_l) + \sigma_l (\Phi_l - \hat{\Phi}_l)}{(\delta \sigma)_l} = -c_p \theta_l \pi \left(\frac{dP}{d\pi}\right)_l, \qquad \text{for } l = 1, \mathrm{LM}. \qquad (45)
$$

Using (39), we see that this last is satisfied if the half thicknesses are given by the following hydrostatic relations:

$$
\begin{aligned}
(\hat{\Phi}_{l+1} - \Phi_l) &= -c_p \theta_l (\hat{P}_{l+1} - P_l), && \text{for } l = 1, \mathrm{LM}, && (46a) \\
(\Phi_l - \hat{\Phi}_l) &= -c_p \theta_l (P_l - \hat{P}_l), && \text{for } l = 2, \mathrm{LM}. && (46b)
\end{aligned}
$$

It is straightforward to verify that these forms of the half thicknesses are consistent with (31), the hydrostatic relations between layers. Furthermore, substituting (46a,b) in the $2(\mathrm{LM}-1)$ relations (44a,b), the latter can be written:

$$c_p(P_{l+1}-P_l)\hat{\theta}_{l+1}=\Phi_l-\Phi_{l+1}, \quad \text{for } l=1,\mathrm{LM}-1,$$

which are identical to (31), and

$$c_p\hat{T}_l=\frac{c_p}{2}(P_l+P_{l-1})\hat{\theta}_l+\frac{1}{2}(\Phi_l+\Phi_{l-1})-\hat{\Phi}_l, \quad \text{for } l=2,\mathrm{LM}, \tag{47}$$

which define the $\mathrm{LM}-1$ interface temperatures we introduced in writing (40).

Using the half thicknesses (46a,b) we can rewrite (41) as:

$$\begin{aligned}\frac{\partial\pi K_l}{\partial t} &= -\nabla\cdot(\pi\mathbf{v}_lK_l)-\frac{1}{2}\frac{1}{(\delta\sigma)_l}\left((\pi\dot{\sigma})_{l+1}\mathbf{v}_{l+1}\cdot\mathbf{v}_l-(\pi\dot{\sigma})_l\mathbf{v}_l\cdot\mathbf{v}_{l-1}\right)\\ &\quad-\nabla(\pi\mathbf{v}_l\Phi_l)-\left(\frac{\delta(\hat{\Phi}\pi\dot{\sigma})}{\delta\sigma}\right)_l-\left(\frac{\delta(\Phi\sigma)}{\delta\sigma}\right)_l\frac{\partial\pi}{\partial t}-g\mathbf{v}_l\cdot\left(\frac{\delta\mathcal{T}}{\delta\sigma}\right)_l\\ &\quad\boxed{-c_p\theta_l\pi\left[\frac{(\pi\dot{\sigma})_{l+1}(\hat{P}_{l+1}-P_l)+(\pi\dot{\sigma})_l(P_l-\hat{P}_l)}{\pi(\delta\sigma)_l}+\left(\frac{dP}{d\pi}\right)_l\left(\frac{\partial\pi}{\partial t}+\mathbf{v}_l\cdot\nabla\pi\right)\right],}\end{aligned} \tag{48}$$

where the boxed term again corresponds to $-(\pi\omega\alpha)_l$. Using (39), this term can be written as:

$$\begin{aligned}(\pi\omega\alpha)_l &= c_p\theta_l\pi\left(\frac{dP}{d\pi}\right)_l\left[\frac{(\pi\dot{\sigma})_{l+1}(\hat{P}_{l+1}-P_l)+(\pi\dot{\sigma})_l(P_l-\hat{P}_l)}{\sigma_{l+1}(\hat{P}_{l+1}-P_l)+\sigma_l(P_l-\hat{P}_l)}+\left(\frac{\partial\pi}{\partial t}+\mathbf{v}_l\cdot\nabla\pi\right)\right]\\ &= \frac{c_p\theta_l\pi}{\tilde{\sigma}_l}\left(\frac{dP}{d\pi}\right)_l\left[\frac{(\pi\dot{\sigma})_{l+1}(\hat{P}_{l+1}-P_l)+(\pi\dot{\sigma})_l(P_l-\hat{P}_l)}{\hat{P}_{l+1}-\hat{P}_l}+\tilde{\sigma}_l\left(\frac{\partial\pi}{\partial t}+\mathbf{v}_l\cdot\nabla\pi\right)\right].\end{aligned} \tag{49}$$

Here we have defined the quantity $\tilde{\sigma}$ as:

$$\tilde{\sigma}_l=\frac{\sigma_{l+1}(\hat{P}_{l+1}-P_l)+\sigma_l(P_l-\hat{P}_l)}{\hat{P}_{l+1}-\hat{P}_l}, \tag{50}$$

which is an interpolation of σ to the layers. The term in brackets on the right-hand side of (49) is a discrete form of ω_l. Clearly, the corresponding α_l is:

$$\alpha_l=\frac{c_p\theta_l}{\tilde{\sigma}_l}\left(\frac{dP}{d\pi}\right)_l.$$

Note that the ω_l obtained from (49) is defined at the layers, not at the interface levels where $\dot{\sigma}_l$ is defined.

Multiplying (40) and (41) by $(\delta\sigma)_l$, summing over all layers, and integrating over the horizontal, we obtain the vertically discrete form of the total energy equation:

$$\frac{\partial}{\partial t}\int_S\sum_{l=1}^{\mathrm{LM}}\pi(c_pT_l+K_l+\Phi_s)(\delta\sigma)_l ds=\int_S\sum_{l=1}^{\mathrm{LM}}\left[\pi\mathcal{Q}_l-g\mathbf{v}_l\cdot\left(\frac{\delta\mathcal{T}}{\delta\sigma}\right)_l\right](\delta\sigma)_l\,ds.$$

4.4 The Vertically Integrated Pressure Gradient Force

The discrete form of the vertically integrated pressure gradient force is:

$$\begin{aligned}\sum_{l=1}^{\mathrm{LM}} \pi (\nabla_p \Phi)_l (\delta\sigma)_l &= \sum_{l=1}^{\mathrm{LM}} \pi \left[\nabla \Phi_l + c_p \theta_l \left(\frac{dP}{d\pi} \right)_l \nabla \pi \right] (\delta\sigma)_l \\ &= \sum_{l=1}^{\mathrm{LM}} \left[\nabla(\pi \Phi_l) - \Phi_l \nabla \pi + c_p \theta_l \pi \left(\frac{dP}{d\pi} \right)_l \nabla \pi \right] (\delta\sigma)_l .\end{aligned}$$

Using (45), the identity (42) can be rewritten:

$$\Phi_l = \left(\frac{\delta(\Phi\sigma)}{\delta\sigma} \right)_l + c_p \theta_l \pi \left(\frac{dP}{d\pi} \right)_l .$$

Thus,

$$\begin{aligned}\sum_{l=1}^{\mathrm{LM}} \pi (\nabla_p \Phi)_l (\delta\sigma)_l &= \nabla \left[\sum_{l=1}^{\mathrm{LM}} (\pi \Phi_l)(\delta\sigma)_l \right] - \Phi_s \nabla \pi \\ &= \nabla \left[\sum_{l=1}^{\mathrm{LM}} \pi (\Phi_l - \Phi_s)(\delta\sigma)_l \right] + \pi \nabla \Phi_s ,\end{aligned}$$

which is in the same form as (24).

5 Horizontal Differencing

5.1 Latitude-Longitude Coordinates

In section 2 the continuous equations were written in vector notation. In this section we rewrite the equations as used in the code, in component notation in spherical coordinates. Let ϕ be the latitude and λ the longitude. The differential elements of arclength along latitude circles and meridians are:

$$dx = a \cos\phi \, d\lambda \tag{51}$$

$$dy = a \ d\phi, \tag{52}$$

where a is the radius of the globe. The differential element of surface area on the sphere is:

$$ds = a^2 \cos\phi \, d\lambda \, d\phi. \tag{53}$$

The gradient operator is:

$$\nabla = \frac{\vec{\lambda}}{a \cos\phi} \frac{\partial}{\partial \lambda} + \frac{\vec{\phi}}{a} \frac{\partial}{\partial \phi}, \tag{54}$$

and the divergence and curl of a horizontal vector, say $\mathbf{v}$, are:

$$\nabla \cdot \mathbf{v} = \frac{1}{a^2 \cos\phi} \left(\frac{\partial a\, u}{\partial \lambda} + \frac{\partial a \cos\phi\, v}{\partial \phi} \right) \tag{55}$$

and

$$\nabla \times \mathbf{v} = \frac{1}{a^2 \cos\phi} \left(\frac{\partial a\, v}{\partial \lambda} - \frac{\partial a \cos\phi\, u}{\partial \phi} \right), \tag{56}$$

where $\vec{\lambda}$ and $\vec{\phi}$ are the horizontal unit vectors, and u and v are the zonal and meridional components of $\mathbf{v}$ in the (λ, ϕ) coordinate system.

In the code we allow the pole of the spherical coordinate system used for the computations to be displaced relative to the geographical pole. If we let (λ, ϕ) denote longitude and latitude on the computational coordinate system, let $(\tilde{\lambda}, \tilde{\phi})$ denote geographical longitude and latitude. The relation between the two coordinate systems is fully determined by specifying the coordinates of the geographical North Pole in the computational coordinate, which we denote by $(\lambda_{NP}, \phi_{NP})$, and a third parameter, λ_0, which represents a rotation about the geographical pole. The relation between geographical and computational axes is shown schematically in figure 2. Using these parameters, the two systems are related by:

$$\begin{aligned}
\sin\tilde{\phi} &= \cos\phi_{NP}\cos\phi\cos(\lambda - \lambda_{NP}) + \sin\phi_{NP}\sin\phi, && \text{(57a)}\\
\cos(\tilde{\lambda} + \lambda_0)\cos\tilde{\phi} &= \sin\phi_{NP}\cos\phi\cos(\lambda - \lambda_{NP}) - \cos\phi_{NP}\sin\phi, && \text{(57b)}\\
\sin(\tilde{\lambda} + \lambda_0)\cos\tilde{\phi} &= \cos\phi\sin(\lambda - \lambda_{NP}), && \text{(57c)}
\end{aligned}$$

or

$$\begin{aligned}
\sin\phi &= \cos\phi_{NP}\cos\tilde{\phi}\cos(\tilde{\lambda} + \lambda_0 - \pi) + \sin\phi_{NP}\sin\tilde{\phi}, && \text{(58a)}\\
\cos(\lambda + \pi - \lambda_{NP})\cos\phi &= \sin\phi_{NP}\cos\tilde{\phi}\cos(\tilde{\lambda} + \lambda_0 - \pi) - \cos\phi_{NP}\sin\tilde{\phi}, && \text{(58b)}\\
\sin(\lambda + \pi - \lambda_{NP})\cos\phi &= \cos\tilde{\phi}\sin(\tilde{\lambda} + \lambda_0 - \pi). && \text{(58c)}
\end{aligned}$$

Note that these transformations can be inverted by making the exchanges:

$$\begin{aligned}
(\lambda, \phi) &\iff (\tilde{\lambda}, \tilde{\phi}), && \text{(59a)}\\
\lambda_{NP} &\iff \pi - \lambda_0. && \text{(59b)}
\end{aligned}$$

The code assumes that all input variables are on the computational coordinate system, and that the input u and v wind components are also along the computational coordinates. It makes the same assumptions for the output variables. With these assumptions, the only effect on the code of displacing the geographical pole away from the computational pole is to modify the Coriolis parameter:

$$f = \quad 2\Omega\sin\tilde{\phi} = 2\Omega\left(\cos\phi_{NP}\cos\phi\cos(\lambda - \lambda_{NP}) + \sin\phi_{NP}\sin\phi\right), \tag{60}$$

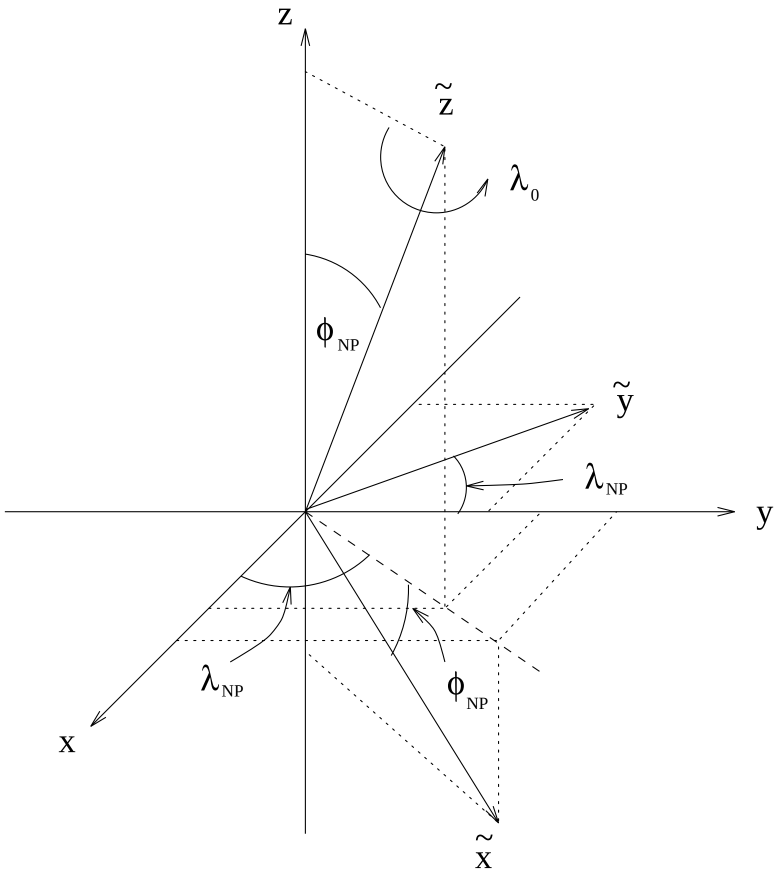

Figure 2: The geographical and computational coordinate axes.

where Ω is the planet's rotation rate. Although there is no other reference to geographical coordinates within the dynamical core, it is generally necessary to transform between the two grids when initializing a run or recording results in geographical coordinates. In addition to interpolation, this requires transforming the velocity components between the two systems. If we let χ denote the local angle between the computational and geographical coordinates, the two sets of velocity components are related by

$$u = \cos\chi\,\tilde{u} - \sin\chi\,\tilde{v}, \tag{61a}$$
$$v = \sin\chi\,\tilde{u} + \cos\chi\,\tilde{v}, \tag{61b}$$

and

$$\tilde{u} = \cos\chi\,u + \sin\chi\,v, \tag{62a}$$
$$\tilde{v} = \cos\chi\,v - \sin\chi\,u. \tag{62b}$$

The angle χ may be obtained from the relations:

$$\cos\tilde{\phi}\cos\chi = \cos\phi\,\sin\phi_{NP} - \cos(\lambda-\lambda_{NP})\,\cos\phi_{NP}\sin\phi, \tag{63a}$$

$$\cos\tilde{\phi}\sin\chi = \cos\phi_{NP}\,\sin(\lambda-\lambda_{NP}). \tag{63b}$$

5.2 The Horizontal Grid

The computational domain consists of a longitude sector extending from pole to pole, with cyclic boundary conditions applied in longitude. The size of the sector is determined by specifying the $\mathcal{N}$-fold symmetry on the sphere. If $\mathcal{N}=1$, the domain is the full globe. Smaller sectors ($\mathcal{N}>1$) can be specified only if the coordinate pole and the geographical pole coincide. The grid divides this domain into JM latitude belts of width $(\Delta\phi)_j$, $j=1,\mathrm{JM}$, and IM zonal sectors of width $(\Delta\lambda)_i$, $i=1,\mathrm{IM}$.

We will start by defining the grid (λ_i,ϕ_j):

$$\phi_0 = -\frac{\pi}{2};\qquad \phi_j = \phi_{j-1}+(\Delta\phi)_j,\quad \text{for } j=1,\mathrm{JM};\qquad \phi_{\mathrm{JM}}=\frac{\pi}{2}; \tag{64}$$

and

$$\lambda_1 = -\frac{\pi}{\mathcal{N}};\qquad \lambda_{i+1} = \lambda_i+(\Delta\lambda)_i,\quad \text{for } i=1,\mathrm{IM};\qquad \lambda_{\mathrm{IM}+1}=\frac{\pi}{\mathcal{N}}. \tag{65}$$

Obviously, the $(\Delta\lambda)_i$ and $(\Delta\phi)_j$ must be specified so that:

$$\sum_{i=1}^{\mathrm{IM}}(\Delta\lambda)_i = \frac{2\pi}{\mathcal{N}} \quad\text{and}\quad \sum_{j=1}^{\mathrm{JM}}(\Delta\phi)_j = \pi.$$

The prognostic variables are located on an Arakawa C grid. The pressure, temperature, and all tracers are located at the points (λ_i,ϕ_j), for all i and for $j=1,\mathrm{JM}-1$, which excludes the poles. We will refer to these as the "p-points." The "u-points," at which the zonal wind components are defined, are located between the "p-points" and on the same latitude circles, while "v-points" are located between "p-points" and on the same meridians. The vorticity is defined at the "ζ-points," on the same latitude circles as v and on the same meridians as u. In addition, the two pole points are considered both v- and ζ-points. This arrangement is shown schematically in figure 3, which also shows the relation of the grid intervals to the staggered variables and the indexing convention. Note that $(\Delta\lambda)_i$ is defined at the u-points and $(\Delta\phi)_j$ at the v-points. Variables defined at p-points are indexed the same as the u-point variables half a grid interval to the *east*, the v-point variables half a grid interval to the *south*, and the ζ-point variables to the *southeast*. With this convention, we define the averaging operators as:

$$\text{At the p-points}\ \begin{cases} (\overline{u}^i)_{i,j} = \frac{1}{2}(u_i+u_{i-1})_j \\ (\overline{v}^j)_{i,j} = \frac{1}{2}(v_j+v_{j+1})_i \end{cases}$$

$$
(\Delta\phi)_j \left\{ \begin{array}{ccc}
\multicolumn{3}{c}{\overbrace{\hphantom{p_{i,j} \quad u_{i,j} \quad p_{i+1,j}}}^{(\Delta\lambda)_i}} \\
p_{i,j} & u_{i,j} & p_{i+1,j} \\
 & & \\
v_{i,j} & \zeta_{i,j} & v_{i+1,j} \\
 & & \\
p_{i,j-1} & u_{i,j-1} & p_{i+1,j-1}
\end{array} \right.
$$

Figure 3: Position of the variables on the C-grid and the indexing convention.

$$
\text{At the } u\text{-points} \left\{ \begin{array}{lcl}
(\overline{p}^{i})_{i,j} & = & \frac{1}{2}(p_i + p_{i+1})_j \\
(\overline{\zeta}^{j})_{i,j} & = & \frac{1}{2}(\zeta_j + \zeta_{j+1})_i
\end{array} \right.
$$

and similarly for u and v at the ζ-points, and p and ζ at the v-points. The difference operators, $(\delta_i u)$, $(\delta_i p)$, etc., are defined analogously. The grid intervals of arclength associated with the interior points are defined as:

$$
\begin{aligned}
(\Delta^u x)_{i,j} &= a \cos\phi_j (\Delta\lambda)_i, && \text{for } j = 1, \mathrm{JM}-1, && \mathbf{(66a)} \\
(\Delta^p x)_{i,j} &= (\overline{\Delta^u x}^{i})_{i,j}, && \text{for } j = 1, \mathrm{JM}-1, && \mathbf{(66b)} \\
(\Delta^v x)_{i,j} &= (\overline{\Delta^p x}^{j})_{i,j}, && \text{for } j = 2, \mathrm{JM}-1, && \mathbf{(66c)}
\end{aligned}
$$

$$
\begin{aligned}
(\Delta^v y)_j &= a(\Delta\phi)_j, && \text{for } j = 1, \mathrm{JM}, && \mathbf{(67a)} \\
(\Delta^p y)_j &= (\overline{\Delta^v y}^{j})_j, && \text{for } j = 2, \mathrm{JM}-2, && \mathbf{(67b)} \\
(\Delta^u y)_j &= (\Delta^p y)_j, && \text{for } j = 1, \mathrm{JM}-1. && \mathbf{(67c)}
\end{aligned}
$$

These are shown schematically in figure 4 for the interior of the grid. The intervals $(\Delta^u x)_{i,0}$, $(\Delta^u x)_{i,\mathrm{JM}}$, $(\Delta^p x)_{i,0}$, $(\Delta^p x)_{i,\mathrm{JM}}$, $(\Delta^u y)_0$, $(\Delta^u y)_{\mathrm{JM}}$, $(\Delta^p y)_0$, $(\Delta^p y)_{\mathrm{JM}}$, $(\Delta^v y)_1$, and $(\Delta^v y)_{\mathrm{JM}}$ do not appear in the equations. The remaining intervals are special cases at the poles:

$$
\begin{aligned}
(\Delta^v x)_{i,1} &= 0, && \mathbf{(68a)} \\
(\Delta^v x)_{i,\mathrm{JM}} &= 0, && \mathbf{(68b)}
\end{aligned}
$$

$$(\Delta^p y)_1 = a\,[(\Delta\phi)_1 + \frac{1}{2}(\Delta\phi)_2], \tag{68c}$$

$$(\Delta^p y)_{\mathrm{JM}-1} = a\,[(\Delta\phi)_{\mathrm{JM}} + \frac{1}{2}(\Delta\phi)_{\mathrm{JM}-1}]. \tag{68d}$$

The grid area elements are:

$$(\Delta_p^2)_{i,j} = (\overline{\Delta^v x}^j)_{i,j}(\Delta^p y)_j, \quad \text{for } j = 2, \mathrm{JM}-2, \tag{69a}$$

$$(\Delta_u^2)_{i,j} = (\Delta^u x)_{i,j}(\Delta^u y)_j, \quad \text{for } j = 1, \mathrm{JM}-1, \tag{69b}$$

$$(\Delta_v^2)_{i,j} = (\Delta^v x)_{i,j}(\Delta^v y)_j, \quad \text{for } j = 1, \mathrm{JM}, \tag{69c}$$

$$(\Delta_\zeta^2)_{i,j} = (\overline{\Delta_p^2}^{ij})_{i,j}, \quad \text{for } j = 2, \mathrm{JM}-1, \tag{69d}$$

and at the poles

$$(\Delta_p^2)_{i,1} = (\Delta^p x)_{i,1}(\Delta^v y)_{i,1}, \tag{69e}$$

$$(\Delta_p^2)_{i,\mathrm{JM}-1} = (\Delta^p x)_{i,\mathrm{JM}-1}(\Delta^v y)_{i,\mathrm{JM}}, \tag{69f}$$

$$(\Delta_\zeta^2)_1 = \frac{1}{2}\left[\frac{1}{\mathrm{IM}}\sum_{i=1}^{\mathrm{IM}}(\Delta_p^2)_{i,1}\right], \tag{69g}$$

$$(\Delta_\zeta^2)_{\mathrm{JM}} = \frac{1}{2}\left[\frac{1}{\mathrm{IM}}\sum_{i=1}^{\mathrm{IM}}(\Delta_p^2)_{i,\mathrm{JM}-1}\right]. \tag{69h}$$

5.3 The Continuity Equation

We use a simple centered second-order form of the continuity equation:

$$\frac{\partial \pi_{i,j}}{\partial t} = -\frac{1}{(\Delta_p^2)_{i,j}}[\delta_i u_l^* + \delta_j v_l^*]_{i,j} - \left(\frac{\delta_l(\pi\dot{\sigma})}{\delta_l \sigma}\right)_{i,j,l}, \tag{70}$$

where u^* and v^* are the mass fluxes

$$u^*_{i,j,l} = (\Delta^u y)_j(\overline{\pi}^i\, u_l)_{i,j}, \quad \text{for } j = 1, \mathrm{JM}-1, \tag{71}$$

$$v^*_{i,j,l} = (\Delta^v x)_{i,j}(\overline{\pi}^j v_l)_{i,j}, \quad \text{for } j = 1, \mathrm{JM}. \tag{72}$$

Summing (70) we have:

$$\frac{\partial \pi_{i,j}}{\partial t} = \boxed{-\sum_{\ell=1}^{\mathrm{LM}}\frac{1}{(\Delta_p^2)_{i,j}}[\delta_i u_\ell^* + \delta_j v_\ell^*]_{i,j}(\delta\sigma)_\ell} \tag{73}$$

and

$$(\pi\dot{\sigma})_{i,j,l+1} = -\sigma_{l+1}\frac{\partial \pi_{i,j}}{\partial t} - \sum_{\ell=1}^{l}\frac{1}{(\Delta_p^2)_{i,j}}[\delta_i u_\ell^* + \delta_j v_\ell^*]_{i,j}(\delta\sigma)_\ell, \qquad \text{for } l = 1, \mathrm{LM}-1, \tag{74}$$

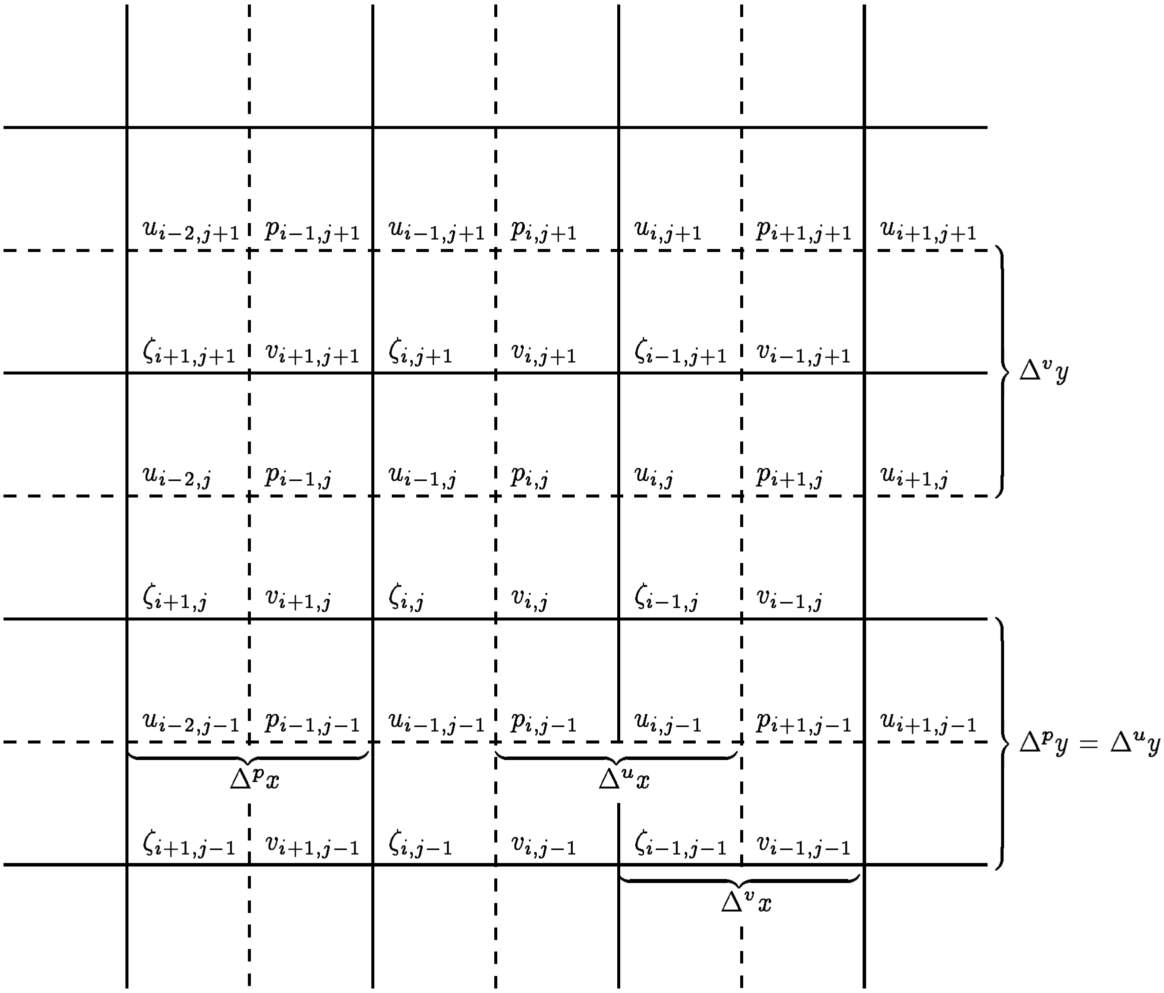

Figure 4: The horizontal C-grid, with the indexing convention used in the text and the code.

which are the forms used in the code. The boxed term in (73) is the dynamical tendency of π computed by the core. Although there should be no other contributions to the π tendency, the code adds the dynamical tendency to the π increment. Increments of the surface pressure (if any) passed to the core are not included in the $\frac{\partial \pi_{i,j}}{\partial t}$ that appears in (74); however, they can enter the calculation in the case of economical explicit differencing described below.

We note that from (68a,b), $v^*_{i,1} = v^*_{i,\mathrm{JM}} = 0$. Using these and cyclic conditions in longitude, the global sum of the divergence vanishes, and we have:

$$\sum_l (\delta_l \sigma) \sum_i \sum_j (\Delta_p^2)_{i,j} \frac{\partial \pi_{i,j}}{\partial t} = \sum_i \sum_j (\Delta_p^2)_{i,j} \frac{\partial \pi_{i,j}}{\partial t} = 0. \tag{75}$$

5.4 The Thermodynamic Equation

We are using the simple second-order, square-conserving (in the horizontal) form of the potential temperature equation:

$$\frac{\partial (\pi \theta_l)_{i,j}}{\partial t} = \boxed{ -\frac{1}{(\Delta_p^2)_{i,j}} [\delta_i (u^* \overline{\theta}^i)_l + \delta_j (v^* \overline{\theta}^j)_l]_{i,j} - \left(\frac{\delta_l (\pi \dot{\sigma}\, \hat{\theta})}{\delta_l \sigma} \right)_{i,j,l} } + \left(\frac{\pi Q_l}{c_p P_l} \right)_{i,j}, \tag{76}$$

where the $\hat{\theta}$ are given by (28). The boxed quantity in (76) is the dynamical tendency added by the core to the $\pi\theta$ increment. Note that it is a mass-weighted tendency. Taking the mass- and area-weighted sum over the domain gives:

$$\sum_l (\delta_l \sigma)_l \sum_i \sum_j (\Delta_p^2)_{i,j} \frac{\partial (\pi \theta_l)_{i,j}}{\partial t} = \sum_l (\delta_l \sigma)_l \sum_i \sum_j (\Delta_p^2)_{i,j} \left(\frac{\pi Q_l}{c_p P_l} \right)_{i,j}. \tag{77}$$

5.4.1 Energy conservation and the thermodynamic equation

Multiplying (76) by $(\Delta_p^2 \, c_p P_l)_{i,j}$ and summing over the horizontal we have:

$$\begin{aligned} \sum_i \sum_j (\Delta_p^2)_{i,j} \left[\frac{\partial (\pi c_p T_l)}{\partial t} - c_p \theta_l \pi \left(\frac{dP_l}{d\pi} \right) \frac{\partial \pi}{\partial t} \right]_{i,j} &= \sum_i \sum_j \left(\Delta_p^2 \, \pi Q_l \right)_{i,j} \\ + \sum_i \sum_j c_p \theta_{i,j,l} \left[\overline{(u^* \delta_i P)_l}^i + \overline{(v^* \delta_j P)_l}^j \right]_{i,j} &- \sum_i \sum_j (\Delta_p^2)_{i,j} \left[c_p P_l \left(\frac{\delta_l (\pi \dot{\sigma}\, \hat{\theta})}{\delta_l \sigma} \right)_l \right]_{i,j}. \end{aligned} \tag{78}$$

In obtaining the first term on the second line, we have used the relations:

$$\sum_i a_i \delta_i b = -\sum_i b_i \delta_i a, \qquad \sum_i \delta_i a = 0, \qquad \sum_i a_i \overline{b}^i = \sum_i b_i \overline{a}^i, \tag{79}$$

and similar relations for j with the polar boundary conditions properly accounted for. The second term on the second line of (78) does not involve the horizontal differencing and so can be manipulated like the analogous term in the first line of (40) to obtain a form like that in (41). Then using (44) and taking the mass-weighted sum over all layers we have:

$$\begin{aligned}
&\sum_l (\delta_l\sigma)_l \sum_i \sum_j (\Delta_p^2)_{i,j} \frac{\partial(\pi c_p T_l)_{i,j}}{\partial t} \\
&\quad= \sum_l (\delta_l\sigma)_l \sum_i \sum_j \left(\Delta_p^2 \pi \mathcal{Q}_l\right)_{i,j} + \sum_l (\delta_l\sigma)_l \sum_i \sum_j (\Delta_p^2 c_p \theta_l \pi)_{i,j} \\
&\qquad \times \left\{ \left[\frac{\dot{\sigma}_{l+1}(\hat{P}_{l+1} - P_l) + \dot{\sigma}_l(P_l - \hat{P}_l)}{\pi(\delta_l\sigma)_l} \right] + \left[\left(\frac{dP_l}{d\pi}\right) \frac{\partial\pi}{\partial t} + \frac{(\overline{(u^*\delta_i P)_l}^i + \overline{(v^*\delta_j P)_l}^j)}{(\pi\,\Delta_p^2)} \right] \right\}_{i,j}
\end{aligned} \tag{80}$$

5.5 The Tracer Equations

We are currently using the same horizontal advection scheme for tracers as for potential temperature advection:

$$\frac{\partial(\pi q_l^{(k)})_{i,j}}{\partial t} = -\frac{1}{(\Delta_p^2)_{i,j}} \left[\delta_i(u^* \overline{q^{(k)}}^i)_l + \delta_j(v^* \overline{q^{(k)}}^j)_l \right]_{i,j} - \left(\frac{\delta_l(\pi\dot{\sigma}\,\hat{q}^{(k)})}{\delta_l\sigma} \right)_{i,j,l} + \left(\pi \mathcal{S}_l^{(k)}\right)_{i,j}, \tag{81}$$

where the $\hat{q}^{(k)}$ are given by (37). Summing over the domain we have

$$\sum_l (\delta_l\sigma) \sum_i \sum_j (\Delta_p^2)_{i,j} \frac{\partial(\pi q_l^{(k)})_{i,j}}{\partial t} = \sum_l (\delta_l\sigma) \sum_i \sum_j (\Delta_p^2)_{i,j} \left(\pi \mathcal{S}_l^{(k)}\right)_{i,j}. \tag{82}$$

5.6 The Momentum Equation

The differencing of the momentum equation is patterned after that of the UCLA model. For the vertical advection term and the pressure gradient force we use a straightforward energy-conserving form. For the inertial terms a fourth-order version of the form of the Sadourney scheme used by Burridge and Haseler (1977). To derive this fourth-order scheme, we followed a procedure similar to that Takano and Wurtele (1982) used to obtain a fourth-order version of the Arakawa and Lamb (1981) scheme. The resulting scheme is somewhat simpler than that of Takano and Wurtele and retains most of the conservation advantages of the Arakawa-Lamb scheme.

5.6.1 The discrete equations in component form

We begin by writing the equations in a general energy-conserving form similar to that used by Arakawa and Lamb (1981):

$$
\begin{aligned}
\frac{\partial u_{i,j,l}}{\partial t} &= \frac{1}{(\Delta^u x)_{i,j}} \Big[\alpha_{i,j} v^*_{i+1,j+1} + \beta_{i,j} v^*_{i,j+1} + \gamma_{i,j} v^*_{i,j} + \delta_{i,j} v^*_{i+1,j} \\
&\qquad + \nu_{i,j} u^*_{i,j-1} - \nu_{i,j+1} u^*_{i,j+1} - \epsilon_{i+1,j} u^*_{i+1,j} + \epsilon_{i,j} u^*_{i-1,j}\Big]_l \\
&\quad - \frac{1}{(\overline{\pi}^i)_{i,j} (\delta_l \sigma)_l} \frac{1}{2} \left[\overline{(\pi\dot\sigma)}^i_l (u_l - u_{l-1}) + \overline{(\pi\dot\sigma)}^i_{l+1} (u_{l+1} - u_l)\right]_{i,j} \\
&\quad - \frac{1}{(\Delta^u x)_{i,j}} \left[\delta_i(\Phi_l + K_l) + c_p \overline{\theta_l \left(\frac{dP}{d\pi}\right)_l \delta_i \pi}^i\right]_{i,j} - \frac{g}{(\overline{\pi}^i)_{i,j}} \left(\frac{\delta_l \mathcal{T}_\lambda}{\delta_l \sigma}\right)_{i,j,l}, \quad \text{for } j = 1, \mathrm{JM}-1,
\end{aligned} \tag{83}
$$

$$
\begin{aligned}
\frac{\partial v_{i,j,l}}{\partial t} &= -\frac{1}{(\Delta^v y)_j} \Big[\alpha_{i-1,j-1} u^*_{i-1,j-1} + \beta_{i,j-1} u^*_{i,j-1} + \gamma_{i,j} u^*_{i,j} + \delta_{i-1,j} u^*_{i-1,j} \\
&\qquad + \mu_{i,j} v^*_{i+1,j} - \mu_{i-1,j} v^*_{i-1,j} - \varphi_{i,j} v^*_{i,j+1} + \varphi_{i,j-1} v^*_{i,j-1}\Big]_l \\
&\quad - \frac{1}{(\overline{\pi}^j)_{i,j} (\delta_l \sigma)_l} \frac{1}{2} \left[\overline{(\pi\dot\sigma)}^j_l (v_l - v_{l-1}) + \overline{(\pi\dot\sigma)}^j_{l+1} (v_{l+1} - v_l)\right]_{i,j} \\
&\quad - \frac{1}{(\Delta^v y)_j} \left[\delta_j(\Phi_l + K_l) + c_p \overline{\theta_l \left(\frac{dP}{d\pi}\right)_l \delta_j \pi}^j\right]_{i,j} - \frac{g}{(\overline{\pi}^j)_{i,j}} \left(\frac{\delta_l \mathcal{T}_\phi}{\delta_l \sigma}\right)_{i,j,l}, \quad \text{for } j = 2, \mathrm{JM}-1.
\end{aligned} \tag{84}
$$

Here the α, β, γ, δ, ϵ, φ, ν, and μ are linear combinations of neighboring potential vorticities. The ν and μ terms were added to the original Arakawa-Lamb formulation by Takano and Wurtele to expand the stencil enough to be able to require fourth-order accuracy. The potential vorticity at interior points is defined as

$$\eta_{i,j,l} = \frac{(\Delta^2_\zeta)_{i,j}(f_{i,j} + \zeta_{i,j,l})}{(\overline{\pi \Delta^2_p}^{ij})_{i,j}}, \quad \text{for } j = 2, \mathrm{JM}-1, \tag{85}$$

where the relative vorticity is given by

$$\zeta_{i,j,l} = \frac{1}{(\Delta^2_\zeta)_{i,j}} \left[(\Delta^v y)_j (\delta_i v)_{i,j,l} - (\delta_j(\Delta^u x\, u_l))_{i,j}\right], \quad \text{for } j = 2, \mathrm{JM}-1. \tag{86}$$

At the two poles the potential vorticity is given by:

$$\eta_{1,l} = \frac{(\Delta^2_\zeta)_1 (f_1 + \zeta_{1,l})}{\frac{1}{2}\frac{1}{\mathrm{IM}} \sum_{i=1}^{\mathrm{IM}} (\Delta^2_p \pi)_{i,1}}, \tag{85a}$$

$$\eta_{\mathrm{JM},l} = \frac{(\Delta^2_\zeta)_{\mathrm{JM}} (f_{\mathrm{JM}} + \zeta_{\mathrm{JM},l})}{\frac{1}{2}\frac{1}{\mathrm{IM}} \sum_{i=1}^{\mathrm{IM}} (\Delta^2_p \pi)_{i,\mathrm{JM}-1}}, \tag{85b}$$

where

$$\zeta_{1,l} = -\frac{1}{(\Delta_\zeta^2)_1}\frac{1}{\mathrm{IM}}\sum_{i=1}^{\mathrm{IM}}(\Delta^u x\, u_l)_{i,1}, \tag{86a}$$

$$\zeta_{\mathrm{JM},l} = \frac{1}{(\Delta_\zeta^2)_{\mathrm{JM}}}\frac{1}{\mathrm{IM}}\sum_{i=1}^{\mathrm{IM}}(\Delta^u x\, u_l)_{i,\mathrm{JM}-1}. \tag{86b}$$

In the code, polar values of the vorticities are replicated at all longitudes.

The discrete form of the kinetic energy, K, is presented below.

The discrete form of the Coriolis parameter is obtained by noting that f is the "planetary" vorticity; that is, the part of the absolute vorticity due to the rotation of the reference frame fixed to the planet. The velocity components of the rotating frame along the geographical coordinates are:

$$\tilde{u}_p = \Omega a\, \cos\tilde{\phi}, \qquad \tilde{v}_p = 0,$$

and from (61), the components along the computational coordinates are:

$$u_p = \Omega a\, \cos\tilde{\phi}\cos\chi, \qquad v_p = \Omega a\, \cos\tilde{\phi}\sin\chi.$$

On the grid, we first define u_p and v_p at the p-points (and at the poles) and then interpolate to the u- and v-points:

$$(u_p)_{i,j} = \Omega a\, \overline{\cos\tilde{\phi}\cos\chi}^{\,i}, \quad \text{for } j = 1, \mathrm{JM}-1, \tag{87a}$$

and

$$(v_p)_{i,j} = \Omega a\, \overline{\cos\tilde{\phi}\sin\chi}^{\,j}, \quad \text{for } j = 2, \mathrm{JM}-1. \tag{87b}$$

Using the same discretization as for relative vorticity, we substitute these in (86) to obtain:

$$\begin{aligned} f_{i,j} &= \frac{\Omega a}{(\Delta_\zeta^2)_{i,j}}\left[\Delta^v y\, \delta_i\overline{(\cos\tilde{\phi}\sin\chi)}^{\,j} - \delta_j(\Delta^u x\, \overline{\cos\tilde{\phi}\cos\chi}^{\,i})\right]_{i,j}, \qquad \text{for } j = 2, \mathrm{JM}-1, \\ &= \frac{\Omega a}{(\Delta_\zeta^2)_{i,j}}\left[\Delta^v y\, \delta_i(\cos\phi_{NP}\, \overline{\sin(\lambda-\lambda_{NP})}^{\,j})\right. \\ &\qquad \left. -\ \delta_j\left(\Delta^u x\left[\sin\phi_{NP}\,\overline{\cos\phi}^{\,i} - \cos\phi_{NP}\,\overline{\cos(\lambda-\lambda_{NP})\,\sin\phi}^{\,i}\right]\right)\right]_{i,j}, \end{aligned}$$

where we have used (63b). The form used in the code is

$$\begin{aligned} &= \frac{-\Omega a}{(\Delta_\zeta^2)_{i,j}}\left[\sin\phi_{NP}\cos\phi\,\delta_j\Delta^u x\right. \\ &\qquad \left. -\cos\phi_{NP}\left[\Delta^v y\,\delta_i\sin(\lambda-\lambda_{NP}) + \overline{\cos(\lambda-\lambda_{NP})}^{\,i}\,\delta_j(\,\Delta^u x\,\sin\phi)\right]\right]_{i,j}, \end{aligned} \tag{88}$$

which takes into account that in latitude longitude coordinates $(\lambda - \lambda_{NP})$ is independent of j and ϕ is independent of i. The right-hand side of (88) is a discrete form of

$$-\frac{\Omega}{\cos\phi}\left(\sin\phi_{NP}\frac{\partial\cos^2\phi}{\partial\phi} - \cos\phi_{NP}\left[\frac{\partial\sin(\lambda-\lambda_{NP})}{\partial\lambda} + \cos(\lambda-\lambda_{NP})\frac{\partial\cos\phi\sin\phi}{\partial\phi}\right]\right), \quad (89)$$

which reduces to (60). At the poles, we have:

$$\begin{aligned} f_1 &= \frac{-\Omega a}{(\Delta_\zeta^2)_1}\frac{1}{\mathrm{IM}}\sum_{\imath=1}^{\mathrm{IM}}\Big[(\Delta^u x)_{\imath,1}\,(\sin\phi_{NP}\,\cos\phi_1 \\ &\qquad - \cos\phi_{NP}\,\cos(\lambda_\imath - \lambda_{NP})\,\sin\phi_1)\Big], \qquad \textbf{(88a)} \\ f_{\mathrm{JM}} &= \frac{\Omega a}{(\Delta_\zeta^2)_{\mathrm{JM}}}\frac{1}{\mathrm{IM}}\sum_{\imath=1}^{\mathrm{IM}}\Big[(\Delta^u x)_{\imath,\mathrm{JM}-1}\,(\sin\phi_{NP}\,\cos\phi_{\mathrm{JM}-1} \\ &\qquad - \cos\phi_{NP}\,\cos(\lambda_\imath - \lambda_{NP})\,\sin\phi_{\mathrm{JM}-1})\Big], \qquad \textbf{(88b)} \end{aligned}$$

which are obtained by substituting (87a) in (86a,b).

5.6.2 Fourth-order vorticity advection: the choice of $\alpha, \beta, \ldots$

The procedure followed by Takano and Wurtele to obtain a fourth-order version of the Arakawa-Lamb scheme was to 1) form an equation for the second-order difference form of the vorticity, 2) assume that the flow is non-divergent and replace the advecting velocities by second-order differences of the streamfunction, and 3) equate terms in the resulting non-divergent vorticity equations with corresponding terms in the fourth-order Jacobian derived by Arakawa (1966). This procedure gives a scheme that is fourth-order *only* in the advection of a *second-order* vorticity by the *non-divergent* part of the flow. We will follow the same procedure, but without requiring that in the shallow-water equations the potential enstrophy be conserved for a general flow. Rather, we will require enstrophy conservation only for the case of non-divergent flow, as in the Sadourney scheme. We will refer to the resulting scheme as a fourth-order Sadourney.

As pointed out by Arakawa and Lamb (1981), the second-order Sadourney scheme corresponds to

$$\begin{aligned} \alpha_{i,j}^S &= \tfrac{1}{12}(\eta_{i,j+1} + \eta_{i,j} + \eta_{i+1,j+1}), & &\text{for } j = 1, \mathrm{JM}-2, & \textbf{(90a)} \\ \beta_{i,j}^S &= \tfrac{1}{12}(\eta_{i,j+1} + \eta_{i,j} + \eta_{i-1,j+1}), & &\text{for } j = 1, \mathrm{JM}-2, & \textbf{(90b)} \\ \gamma_{i,j}^S &= \tfrac{1}{12}(\eta_{i,j+1} + \eta_{i,j} + \eta_{i-1,j}), & &\text{for } j = 2, \mathrm{JM}-1, & \textbf{(90c)} \\ \delta_{i,j}^S &= \tfrac{1}{12}(\eta_{i,j+1} + \eta_{i,j} + \eta_{i+1,j}), & &\text{for } j = 2, \mathrm{JM}-1, & \textbf{(90d)} \end{aligned}$$

where the j ranges take into account that $v_{i,1}^* = v_{i,\mathrm{JM}}^* = 0$, and so some of the values neighboring the poles are not used. For the Sadourney scheme,

$$\epsilon_{i,j}^S = \varphi_{i,j}^S = 0, \quad (90e)$$

and

$$\nu^S_{i,j} = \mu^S_{i,j} = 0. \tag{90f}$$

Requiring potential enstrophy conservation only for non-divergent flow thus allows us to eliminate the $\epsilon_{i,j}$ and $\varphi_{i,j}$ terms. Dropping these terms is very attractive because we have found them quite troublesome. In three-dimensional calculations with the GCM, we found that they are responsible for much of the problem our implementation of the Arakawa-Lamb scheme had near the poles. These problems were eliminated when we used the second-order Sadourney, and so we used that scheme for Version 1 of the ARIES/GEOS dynamical core. We note that the ν and μ terms, required for fourth-order accuracy, are similar in that they involve u in the u equation and v in the v equation. Indeed we found a similar, though lesser, problem when these terms were included. This problem, however, is easily corrected, as we will discuss in section 5.6.4.

Following the procedure outlined above, Takano and Wurtele found that the following relations must be satisfied to obtain fourth-order accuracy:

$$\begin{aligned}
\alpha_{i,j} &= C_{i+1,j} + \frac{1}{96}\big[16\eta_{i,j+1} + 8(\eta_{i+1,j+1} + \eta_{i,j}) - 3(\eta_{i-1,j+1} + \eta_{i,j+2}) \\
&\quad + (\underline{\eta_{i+1,j-1}} + \underline{\eta_{i+2,j}}) - (\eta_{i-1,j} + \eta_{i,j+1} + \underline{\eta_{i+1,j+2}} + \underline{\eta_{i+2,j+1}})\big] \\
&\quad + \frac{1}{2}(\epsilon + \varphi)_{i+1.j}, \quad \text{for } j = 1, \mathrm{JM} - 2, \qquad (91a)\\
\beta_{i,j} &= -C_{i,j} + \frac{1}{96}\big[16\eta_{i,j+1} + 8(\eta_{i-1,j+1} + \eta_{i,j}) - 3(\eta_{i+1,j+1} + \eta_{i,j+2}) \\
&\quad + (\underline{\eta_{i-1,j-1}} + \underline{\eta_{i-2,j}}) - (\eta_{i+1,j} + \eta_{i,j-1} + \underline{\eta_{i-1,j+2}} + \underline{\eta_{i-2,j+1}})\big] \\
&\quad + \frac{1}{2}(\epsilon + \varphi)_{i.j}, \quad \text{for } j = 1, \mathrm{JM} - 2, \qquad (91b)\\
\gamma_{i,j} &= C_{i,j} + \frac{1}{96}\big[16\eta_{i,j} + 8(\eta_{i-1,j} + \eta_{i,j+1}) - 3(\eta_{i,j-1} + \eta_{i+1,j}) \\
&\quad + (\underline{\eta_{i-2,j+1}} + \underline{\eta_{i-1,j+2}}) - (\underline{\eta_{i-2,j}} + \underline{\eta_{i-1,j-1}} + \eta_{i,j+2} + \eta_{i+1,j+1})\big] \\
&\quad + \frac{1}{2}(\epsilon + \varphi)_{i.j}, \quad \text{for } j = 2, \mathrm{JM} - 1, \qquad (91c)\\
\delta_{i,j} &= -C_{i+1,j} + \frac{1}{96}\big[16\eta_{i,j} + 8(\eta_{i,j+1} + \eta_{i+1,j}) - 3(\eta_{i-1,j} + \eta_{i,j-1}) \\
&\quad + (\underline{\eta_{i+1,j+2}} + \underline{\eta_{i+2,j+1}}) - (\underline{\eta_{i+2,j}} + \underline{\eta_{i+1,j-1}} + \eta_{i,j+2} + \eta_{i-1,j+1})\big] \\
&\quad + \frac{1}{2}(\epsilon + \varphi)_{i+1.j}, \quad \text{for } j = 2, \mathrm{JM} - 1, \qquad (91d)
\end{aligned}$$

$$\nu_{i,j} = \frac{1}{24}(\eta_{i+1,j} - \eta_{i-1,j}), \quad \text{for } j = 1, \mathrm{JM}, \tag{92a}$$

$$\mu_{i,j} = \frac{1}{24}(\eta_{i,j-1} - \eta_{i,j+1}), \quad \text{for } j = 2, \text{JM} - 1, \tag{92b}$$

where the quantities C, ϵ, and ϕ may be any combination of ηs. From (92a), $\nu_{i,1} = \nu_{i,\text{JM}} = 0$, and so terms involving $u^*_{i,1}$ and $u^*_{i,\text{JM}}$ in (83) disappear.

Takano and Wurtele, following the same procedure as Arakawa and Lamb, use the choice of C, ϵ, and ϕ to obtain enstrophy conservation for a general flow. We follow Sadourney by setting

$$\epsilon_{i,j} = \varphi_{i,j} = 0 \tag{93}$$

and thus abandoning exact potential enstrophy conservation for divergent flows. This leaves only C to be determined. Note that the choice of C will only affect α, β, γ, and δ; the quantities ν and μ are the same for all fourth-order schemes.

We will choose C fairly arbitrarily to make the scheme as simple as possible. Figure 5 shows a stencil of the ηs neighboring $u_{i,j}$ and the corresponding α, β, γ, and δ. This stencil covers all the ηs that appear in equations (91a-d). For comparison, we also show the stencils for the second-order Sadourney, as well as the Arakawa-Lamb and Takano-Wurtele schemes. The second-order Sadourney uses only the vorticities within the dashed rectangle in computing α, β, γ, and δ at (i,j). The Arakawa-Lamb and Takano-Wurtele schemes use the vorticities within the hexagonal region—only two more points than the Sadourney scheme. Equations (91a-d) involve and additional *eight* points: the four enclosed in solid squares, which appear underlined in (91a,d), and the four enclosed in dashed squares, which appear underlined in (91b,c).

We first require that C be such that the scheme uses only the Arakawa-Lamb stencil. This is satisfied if

$$C_{i,j} = \hat{C}_{i,j} + \frac{1}{96}\left[(\eta_{i-1,j-1} + \eta_{i-2,j}) - (\eta_{i-1,j+2} + \eta_{i-2,j+1}) + (\eta_{i,j+2} + \eta_{i+1,j+1}) - (\eta_{i,j-1} + \eta_{i+1,j})\right], \tag{94}$$

where $\hat{C}_{i,j}$ depends only on vorticities within the desired stencil. We then choose

$$\hat{C}_{i,j} = \frac{1}{24}\left[(\eta_{i-1,j} + \eta_{i,j+1}) - (\eta_{i-1,j+1} + \eta_{i,j})\right], \tag{95}$$

for which the scheme can be written in the particularly simple form:

$$(\alpha,\beta,\gamma,\delta)_{i,j} = \frac{3}{2}(\alpha,\beta,\gamma,\delta)^S_{i,j} - \frac{1}{2}(\alpha,\beta,\gamma,\delta)^N_{i,j}, \tag{96}$$

where

$$\alpha^N_{i,j} = \frac{1}{12}(\eta_{i+1,j} + \eta_{i,j+2} + \eta_{i-1,j+1}), \quad \text{for } j = 1, \text{JM} - 2, \tag{97a}$$

$$\beta^N_{i,j} = \frac{1}{12}(\eta_{i,j+2} + \eta_{i-1,j} + \eta_{i+1,j+1}), \quad \text{for } j = 1, \text{JM} - 2, \tag{97b}$$

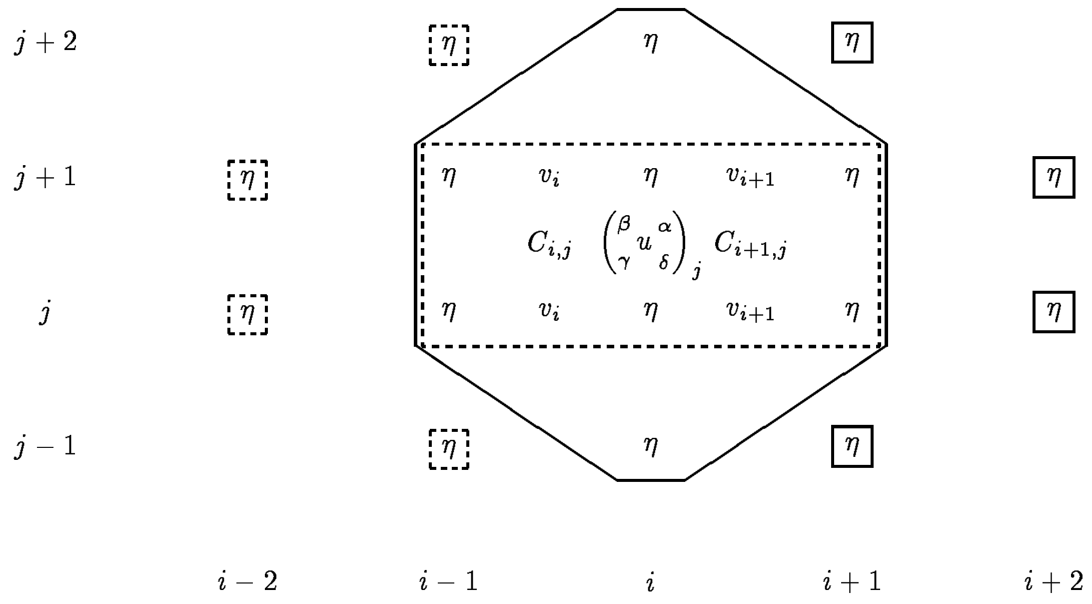

Figure 5: Stencils of ηs used to define the α,β,etc.

$$
\begin{aligned}
\gamma^N_{i,j} &= \frac{1}{12}(\eta_{i,j-1} + \eta_{i+1,j} + \eta_{i-1,j+1}), \quad \text{for } j = 2, \mathrm{JM}-1, && \textbf{(97c)} \\
\delta^N_{i,j} &= \frac{1}{12}(\eta_{i+1,j+1} + \eta_{i,j-1} + \eta_{i-1,j}), \quad \text{for } j = 2, \mathrm{JM}-1. && \textbf{(97d)}
\end{aligned}
$$

5.6.3 Energy conservation and the momentum equation

To form a kinetic energy equation we multiply (83) by $(\Delta^u x\, u^*_l)_{i,j}$ and (84) by $(\Delta^v y)_j\, v^*_{i,j,l}$:

$$
\begin{aligned}
\left[\Delta^2_u \overline{\pi}^i \frac{\partial \frac{1}{2} u_l^2}{\partial t}\right]_{i,j} &= -g\left[\Delta^2_u\, u_l \left(\frac{\delta_l \mathcal{T}_\lambda}{\delta_l \sigma}\right)_l\right]_{i,j} \\
&+ u^*_{i,j,l}\left[\alpha_{i,j} v^*_{i+1,j+1} + \beta_{i,j} v^*_{i,j+1} + \gamma_{i,j} v^*_{i,j} + \delta_{i,j} v^*_{i+1,j}\right]_l \\
&+ u^*_{i,j,l}\left[\nu_{i,j+1} u^*_{i,j+1} - \nu_{i,j} u^*_{i,j-1}\right]_l \\
&- \frac{1}{(\delta_l \sigma)_l}\frac{1}{2}\left[\Delta^2_u\, u_l \left(\overline{(\pi\dot{\sigma})}^i_l (u_l - u_{l-1}) + \overline{(\pi\dot{\sigma})}^i_{l+1}(u_{l+1} - u_l)\right)\right]_{i,j}
\end{aligned}
$$

$$- u^*_{i,j,l}\left[\delta_i(\Phi_l + K_l) + c_p \overline{\theta_l \left(\frac{dP}{d\pi}\right)_l \delta_i \pi}^i\right]_{i,j}, \qquad \text{for } j = 1, \mathrm{JM}-1, \tag{98}$$

$$\begin{aligned}
\left[\Delta^2_v \, \overline{\pi}^j \frac{\partial \frac{1}{2} v_l^2}{\partial t}\right]_{i,j} &= -g\left[\Delta^2_v \, v_l \left(\frac{\delta_l \mathcal{T}_\phi}{\delta_l \sigma}\right)_l\right]_{i,j} \\
&- v^*_{i,j,l}\left[\alpha_{i-1,j-1} u^*_{i-1,j-1} + \beta_{i,j-1} u^*_{i,j-1} + \gamma_{i,j} u^*_{i,j} + \delta_{i-1,j} u^*_{i-1,j}\right]_l \\
&- v^*_{i,j,l}\left[\mu_{i,j} v^*_{i+1,j} - \mu_{i-1,j} v^*_{i-1,j}\right]_l \\
&- \frac{1}{(\delta_l \sigma)_l}\frac{1}{2}\left[\Delta^2_v \, v_l \left(\overline{(\pi\dot{\sigma})}^j_l (v_l - v_{l-1}) + \overline{(\pi\dot{\sigma})}^j_{l+1}(v_{l+1} - v_l)\right)\right]_{i,j} \\
&- v^*_{i,j,l}\left[\delta_j(\Phi_l + K_l) + c_p \overline{\theta_l \left(\frac{dP}{d\pi}\right)_l \delta_j \pi}^j\right]_{i,j}, \qquad \text{for } j = 2, \mathrm{JM}-1.
\end{aligned} \tag{99}$$

The global integral of the kinetic energy tendency at each level can now be obtained by adding (98) and (99) and summing over all i and j. Doing this we have on the left-hand side:

$$\begin{aligned}
& \sum_i \sum_{j=1}^{\mathrm{JM}-1} \left(\Delta^2_u \, \overline{\pi}^i \frac{\partial \frac{1}{2} u_l^2}{\partial t}\right)_{i,j} + \sum_i \sum_{j=2}^{\mathrm{JM}-1} \left(\Delta^2_v \, \overline{\pi}^j \frac{\partial \frac{1}{2} v_l^2}{\partial t}\right)_{i,j} \\
= \quad & \sum_i \sum_{j=1}^{\mathrm{JM}-1} \pi_{i,j} \frac{\partial}{\partial t}\left[\overline{\Delta^2_u \frac{1}{2} u_l^2}^i + \overline{\Delta^2_v \frac{1}{2} v_l^2}^j\right]_{i,j}, \\
= \quad & \sum_i \sum_{j=1}^{\mathrm{JM}-1} (\Delta^2_p)_{i,j} \pi_{i,j} \frac{\partial K^c_{i,j,l}}{\partial t},
\end{aligned} \tag{100}$$

since $(\Delta^2_v)_{i,1} = (\Delta^2_v)_{i,\mathrm{JM}} = 0$. Here K^c is the discrete form of the kinetic energy per unit mass:

$$K^c_{i,j,l} \equiv \frac{1}{(\Delta^2_p)_{i,j}}\left(\overline{\Delta^2_u \frac{1}{2} u_l^2}^i + \overline{\Delta^2_v \frac{1}{2} v_l^2}^j\right)_{i,j}, \quad \text{for } j = 1, \mathrm{JM}-1., \tag{\textbf{101}}$$

We can perform a similar manipulation under the summation of the right-hand side, since in the u equation all reordering is done over i, which is cyclic, and in the v equation, terms at the poles that appear when the sums are reordered as averages at the p-points contain a factor of either v^* or Δ^2_v, which are both zero at $j = 1$ and $j = \mathrm{JM}$.

$$\begin{aligned}
\sum_i \sum_j \left[\frac{\partial}{\partial t}\left(\Delta^2_p \, \pi K^c_l\right)_{i,j} - (\Delta^2_p K^c_l)_{i,j} \frac{\partial \pi_{i,j}}{\partial t}\right] &= -\sum_i \sum_j g\left[\overline{\Delta^2_u \, u_l \left(\frac{\delta_l \mathcal{T}_\lambda}{\delta_l \sigma}\right)_l}^i + \overline{\Delta^2_v \, v_l \left(\frac{\delta_l \mathcal{T}_\phi}{\delta_l \sigma}\right)_l}^j\right]_{i,j} \\
- \textstyle\sum_i \sum_j \quad \frac{1}{(\delta_l \sigma)_l}\frac{1}{2}\Big[\Big((\pi\dot{\sigma})_l \overline{\Delta^2_u \, u_l (u_l - u_{l-1})}^i + (\pi\dot{\sigma})_{l+1} \overline{\Delta^2_u \, u_l (u_{l+1} - u_l)}^i\Big)
\end{aligned}$$

$$+ \left((\pi\dot{\sigma})_l \overline{\Delta_v^2\, v_l(v_l - v_{l-1})}^j + (\pi\dot{\sigma})_{l+1} \overline{\Delta_v^2\, v_l(v_{l+1} - v_l)}^j\right)\Big]_{i,j}$$

$$+ \textstyle\sum_i \sum_j \quad \left[(\Phi_l + K_l)\,(\delta_i u_l^* + \delta_j v_l^*) - c_p \theta_l \left(\frac{dP}{d\pi}\right)_l \left(\overline{u_l^*\, \delta_i \pi}^i + \overline{v_l^*\, \delta_j \pi}^j\right)\right]_{i,j}, \qquad (102)$$

$$\sum_i \sum_j \left[\frac{\partial}{\partial t}\left(\Delta_p^2 \pi K_l^c\right)_{i,j}\right] = \quad -\sum_i \sum_j g \left[\overline{\Delta_u^2\, u_l \left(\frac{\delta_l \mathcal{T}_\lambda}{\delta_l \sigma}\right)_l}^i + \overline{\Delta_v^2\, v_l \left(\frac{\delta_l \mathcal{T}_\phi}{\delta_l \sigma}\right)_l}^j\right]_{i,j}$$

$$+ \textstyle\sum_i \sum_j \quad (\Delta_p^2 K_l^c)_{i,j} \left[\frac{\partial \pi_{i,j}}{\partial t} + \frac{1}{(\Delta_p^2)_{i,j}}(\delta_i u_l^* + \delta_j v_l^*)_{i,j} + \left(\frac{\delta_l(\pi\dot{\sigma})}{\delta_l \sigma}\right)_{i,j,l}\right]$$

$$+ \textstyle\sum_i \sum_j \quad (K_l - K_l^c)_{i,j}(\delta_i u_l^* + \delta_j v_l^*)_{i,j}$$

$$- \textstyle\sum_i \sum_j \quad \frac{1}{(\delta_l \sigma)_l} \frac{1}{2} \Big[\left((\pi\dot{\sigma})_{l+1} \overline{\Delta_u^2\, u_l u_{l+1}}^i - (\pi\dot{\sigma})_l \overline{\Delta_u^2\, u_l u_{l-1}}^i\right)$$

$$+ \left((\pi\dot{\sigma})_{l+1} \overline{\Delta_v^2\, v_l v_{l+1}}^j - (\pi\dot{\sigma})_l \overline{\Delta_v^2\, v_l v_{l-1}}^j\right)\Big]_{i,j}$$

$$- \textstyle\sum_i \sum_j \quad \left[\Delta_p^2\, \Phi_l \left[\frac{\partial \pi}{\partial t} + \left(\frac{\delta_l(\pi\dot{\sigma})}{\delta_l \sigma}\right)_l\right] + c_p \theta_l \left(\frac{dP}{d\pi}\right)_l \left(\overline{u_l^*\, \delta_i \pi}^i + \overline{v_l^*\, \delta_j \pi}^j\right)\right]_{i,j}. \quad (103)$$

The second line of (103) drops out using the continuity equation, and the third line vanishes if we take

$$K = K^c.$$

Note that the α, β, γ, δ, ν, and μ terms do not appear in (103). The α, β, γ, δ terms cancel between the u and v equations when summed over the globe, assuming an appropriate treatment at the poles. This cancellation can be clarified by considering the stencil shown in figures 6.

In figure 6, the α, β, γ, and δ are shown between the us and vs they affect. Each term appears in the equation for the neighboring u multiplied by the neighboring v and in the neighboring v equation multiplied by the neighboring u, but with opposite sign. For example, $\beta_{i,j}$ appears in the $u_{i,j}$ equation multiplied by $v^*_{i,j+1}$, and in the $v_{i,j+1}$ equation (obtained by incrementing j by 1 in (84)) multiplied by $u^*_{i,j}$. (Note that the convention we use here and in the code is that the α, β, γ, δ are indexed the same as the u equation in which they appear.) The ν and μ terms vanish when (98) and (99) are summed over i and j, respectively. The stencil for the ν and μ terms is shown in figure 7. Note that ν and μ are defined at the ζ-points.

Multiplying (103) by $(\delta_l \sigma)_l$, summing over all layers, and using (70), we obtain the following form of the total kinetic energy equation:

$$\sum_l (\delta_l \sigma)_l \sum_i \sum_j \left[\frac{\partial}{\partial t}\left(\Delta_p^2 \pi K_l\right)_{i,j}\right] = -g\mathcal{D}$$

$$\begin{array}{ccccccc} & & & v_{i,j+1} & & & \\ \beta_{i-1,j} & & \alpha_{i-1,j} & & \beta_{i,j} & & \alpha_{i,j} \\ & u_{i-1,j} & & K_{i,j} & & u_{i,j} & \\ \gamma_{i-1,j} & & \delta_{i-1,j} & & \gamma_{i,j} & & \delta_{i,j} \\ & & & v_{i,j} & & & \end{array}$$

Figure 6: Stencil showing the indexing of the α, β, γ, δ factors that appear in the energy conserving form of the inertial terms.

$$-\sum_l (\delta_l\sigma)_l \sum_i \sum_j \left\{ (\Delta_p^2)\,\Phi_l \left[\frac{\partial \pi}{\partial t} + \left(\frac{\delta(\pi\dot{\sigma})}{\delta\sigma}\right)_l\right] + c_p\theta_l \left(\frac{dP}{d\pi}\right)_l \left(\overline{u_l^*\,\delta_i\pi}^i + \overline{v_l^*\,\delta_j\pi}^j\right)\right\}_{i,j}, \quad (104)$$

where $\mathcal{D}$ is the total kinetic energy dissipation:

$$\mathcal{D} = \sum_l (\delta_l\sigma)_l \sum_i \sum_j \left[\overline{\Delta_u^2\, u_l \left(\frac{\delta_l \mathcal{T}_\lambda}{\delta_l\sigma}\right)_l}^i + \overline{\Delta_v^2\, v_l \left(\frac{\delta_l \mathcal{T}_\phi}{\delta_l\sigma}\right)_l}^j\right]_{i,j}.$$

The first term in the curly brackets in (104) involves no horizontal differencing and can be manipulated in the same way as in the horizontally continuous case discussed in section 4.3, equations (41) through (48). Doing this gives

$$\begin{aligned} \frac{\partial}{\partial t}\sum_l (\delta_l\sigma)_l \sum_i\sum_j (\Delta_p^2)_{i,j}\pi_{i,j}\,(K_l+\Phi_s)_{i,j} = -g\mathcal{D} \quad &- \sum_l (\delta_l\sigma)_l \sum_i\sum_j (\Delta_p^2\, c_p\theta_l\pi)_{i,j} \\ \times \left\{ \left[\frac{(\pi\dot{\sigma})_{l+1}(\hat{P}_{l+1}-P_l) + (\pi\dot{\sigma})_l(P_l-\hat{P}_l)}{\pi(\delta_l\sigma)_l}\right] + \left(\frac{dP_l}{d\pi}\right)\left[\frac{\partial\pi}{\partial t} + \frac{\overline{u_l^*\,\delta_i\pi}^i + \overline{v_l^*\,\delta_j\pi}^j}{\pi\,\Delta_p^2}\right]\right\}_{i,j} \quad (105) \end{aligned}$$

Notice that the factors in curly brackets in the conversion terms in (105) and (80) are not identical, and thus the horizontally discrete form of the equations does not conserve energy exactly. The difference stems from the $\theta\left(\frac{dP_l}{d\pi}\right)\nabla\pi$ term in the pressure-gradient force. If this term were discretized as

$$\overline{\theta}^i\,\delta_i P,$$

rather than

$$\overline{\theta\left(\frac{dP}{d\pi}\right)}^i\,\delta_i\pi,$$

$$
\begin{array}{ccccc}
 & u_{i-1,j+1} & & u_{i,j+1} & \\
v_{i-1,j+1} & (\nu,\mu)_{i-1,j+1} & v_{i,j+1} & (\nu,\mu)_{i,j+1} & v_{i+1,j+1} \\
 & u_{i-1,j} & K_{i,j} & u_{i,j} & \\
v_{i-1,j} & (\nu,\mu)_{i-1,j} & v_{i,j} & (\nu,\mu)_{i,j} & v_{i+1,j} \\
 & u_{i-1,j-1} & & u_{i,j-1} &
\end{array}
$$

Figure 7: Stencil showing the indexing of the ν and μ factors that appear in the energy conserving form of the inertial terms.

conservation would be exact. We have not done this because the conserving form does not allows us to maintain the irrotationality constraint on the vertically integrated pressure-gradient force. In any case, we will be abandoning exact energy conservation in applying the polar filter and other modifications described in the following sections. The non-conserving form of the equations also allows us to simplify the implementation of the economical explicit scheme described below.

Comparing (105) with (48), we see that the horizontally discrete form of $(\pi\omega\alpha)_{i,j,l}$ analogous to (49) is

$$
\begin{aligned}
(\pi\omega\alpha)_{i,j,l} = &\left[\frac{c_p\theta_l\pi}{\tilde{\sigma}_l}\left(\frac{dP}{d\pi}\right)_l\right]_{i,j} \\
&\times\left\{\frac{(\pi\dot{\sigma})_{l+1}(\hat{P}_{l+1}-P_l)+(\pi\dot{\sigma})_l(P_l-\hat{P}_l)}{\hat{P}_{l+1}-\hat{P}_l}+\tilde{\sigma}_l\left[\frac{\partial\pi}{\partial t}+\frac{\overline{u_l^*\,\delta_i\pi}^i+\overline{v_l^*\,\delta_j\pi}^j}{\pi\,\Delta_p^2}\right]\right\}_{i,j}, \quad \mathbf{(106)}
\end{aligned}
$$

where $\tilde{\sigma}_{i,j,l}$ is given by (50) evaluated at each grid point. This is the form used to evaluate the ω returned by the code.

5.6.4 Instabilities of the discretized vector invariant form

Hollingsworth-Kållberg instability. The discrete form of the equations presented above suffer from the computational instability discussed by Hollingsworth et al. (1983). This instability is associated with the horizontal differencing of the inertial terms and is common in schemes written in vector-invariant form. It manifests itself as noise with short meridional scales and long zonal scales in regions of strong zonal flow.

Hollingsworth et al. present a heuristic argument suggesting that a spurious source of momentum is producing the instability. To illustrate this argument we consider the one-dimensional shallow-water equations written in vector-invariant form. Ignoring sphericity we have:

$$\begin{aligned}\frac{\partial u}{\partial t} - (f+\zeta)\,v &= 0,\\ \frac{\partial v}{\partial t} + (f+\zeta)\,u &= -g\frac{\partial h}{\partial y} - \frac{\partial}{\partial y}(\frac{1}{2}u^2 + \frac{1}{2}v^2).\end{aligned}$$

Expanding terms in the v equation, we obtain the advective form:

$$\frac{\partial v}{\partial t} + f\,u - \underline{u\frac{\partial u}{\partial y}} = -g\frac{\partial h}{\partial y} - \underline{u\frac{\partial u}{\partial y}} - v\frac{\partial v}{\partial y}.$$

The argument of Hollingsworth et al. is that the underlined terms do not cancel in the discrete form of the equations, resulting in a spurious source of momentum. The following linear system illustrates the effect of having such a term in the equations:

$$\begin{aligned}\frac{\partial u}{\partial t} - f\,v &= 0,\\ \frac{\partial v}{\partial t} + f\,u &= -g\frac{\partial h}{\partial y} - U\frac{\partial u}{\partial y},\\ \frac{\partial h}{\partial t} &= -H\frac{\partial v}{\partial y},\end{aligned}$$

where we have linearized about a uniform zonal flow U and neglected the basic-state gradient of the depth. The dispersion relation for this system is:

$$\sigma^2 = f^2 + gH\,l^2 + \imath\, fUl, \tag{107}$$

where σ is the frequency, l is the wavenumber in y, and $\imath = \sqrt{-1}$. Note that unstable solutions occur when f and U are non-zero.

The simplest way of obtaining cancellation is to modify the form of the kinetic energy that appears on the right-hand side of the momentum equation. Hollingsworth et al. present such a modification for the second-order Sadourney scheme. We will follow a similar approach that is currently being used in the UCLA model to remove the instability from the Arakawa-Lamb scheme. Rather than requiring exact cancellation, this approach only requires that the terms cancel when the equations are linearized in cartesian coordinates. Although a much weaker constraint than exact cancellation, this removes the instability with a smaller modification of the kinetic energy term, and so maintains better conservation.

We wish the discrete form of the inertial terms to satisfy the relation

$$u\zeta = -\frac{1}{2}\frac{\partial u^2}{\partial y},$$

for one-dimensional flow when linearized about a uniform zonal flow. In this case, the discrete form of $u\zeta$ at latitude j is:

$$U\left(\alpha_{j-1} + \beta_{j-1} + \gamma_j + \delta_j\right) = U\,\frac{1}{12}(10\zeta_j + \zeta_{j+1} + \zeta_{j-1}), \tag{108}$$

since

$$\begin{aligned}
\alpha_{j-1} = \beta_{j-1} &= \frac{1}{8}(2\zeta_j + \zeta_{j-1}) - \frac{1}{24}(\zeta_{j-1} + \zeta_j + \zeta_{j+1}), \\
&= \frac{1}{12}\zeta_{j-1} + \frac{5}{24}\zeta_j - \frac{1}{24}\zeta_{j+1}, \\
\gamma_j = \delta_j &= \frac{1}{8}(2\zeta_j + \zeta_{j+1}) - \frac{1}{24}(\zeta_{j-1} + \zeta_j + \zeta_{j+1}), \\
&= \frac{1}{12}\zeta_{j+1} + \frac{5}{24}\zeta_j - \frac{1}{24}\zeta_{j-1}.
\end{aligned}$$

It is worth noting that the quantity $(\alpha_{j-1} + \beta_{j-1} + \gamma_j + \delta_j)$ is independent of the choice of C; thus that choice could not be used to optimize the form of K. Substituting

$$\zeta_j = u_j - u_{j-1}$$

in (108), we have:

$$\begin{aligned}
U\left(\alpha_{j-1} + \beta_{j-1} + \gamma_j + \delta_j\right) &= U\,\frac{1}{12}(10(u_j - u_{j-1}) + u_{j+1} - u_j + u_{j-1} - u_{j-2}), \\
&= U\,\frac{1}{12}((u_{j-1} + 10u_j + u_{j+1}) - (u_{j+1} + 10u_{j-1} + u_{j-2})),
\end{aligned}$$

from which we see that the linearized form of the kinetic energy must be

$$K_j = U\left[\frac{5}{6}u_j + \frac{1}{6}\frac{1}{2}(u_{j-1} + u_{j+1})\right].$$

This is the linearization of

$$K_j = \frac{1}{2}\left[\frac{5}{6}u_j^2 + \frac{1}{6}\tilde{u}_j^2\right],$$

where

$$\tilde{u}_j \equiv \frac{1}{2}(u_{j-1} + u_{j+1}).$$

Putting in the map factors and applying this scheme in both directions, we have:

$$K = \frac{5}{6}K^c + \frac{1}{6}K^s, \tag{109}$$

where

$$K^s_{i,j,l} \equiv \frac{1}{(\Delta_p^2)_{i,j}} \left(\overline{\Delta_u^2 \frac{1}{2} \tilde{u}_l^2}^{i} + \overline{\Delta_v^2 \frac{1}{2} \tilde{v}_l^2}^{j} \right)_{i,j}, \qquad \text{for } j = 2, \mathrm{JM}-2, \tag{110}$$

and

$$\tilde{u}_{i,j,l} = \frac{1}{2}(u_{i,j+1,l} + u_{i,j-1,l}), \tag{111}$$

$$\tilde{v}_{i,j,l} = \frac{1}{2}(v_{i+1,j,l} + v_{i-1,j,l}). \tag{112}$$

At the poles we use the conserving form:

$$K_{i,1,l} = K^c_{i,1,l} \quad \text{and} \quad K_{i,\mathrm{JM}-1,l} = K^c_{i,\mathrm{JM}-1,l}. \tag{113}$$

The ν term at the poles. As discussed above, we found that the ν term given by (92a) tends to produce zonal noise near the poles. This is similar to the problem we had encountered earlier with the ϵ and ϕ terms in Arakawa-Lamb scheme, and seems to be related to the fact that these inertial terms, although conservative, are not acting normal to the flow. The problem, however, is confined to the poles, and the culprit seems to be the ν factor at $j = 2$ and $\mathrm{JM}-1$. We are circumventing this problem by replacing these νs by interpolations between interior and pole values:

$$\nu_{i,2} = \nu_{i,3} \frac{(\Delta^p y)_1}{(\Delta^p y)_1 + (\Delta^p y)_2}, \tag{114a}$$

$$\nu_{i,\mathrm{JM}-1} = \nu_{i,J-2} \frac{(\Delta^p y)_{\mathrm{JM}-1}}{(\Delta^p y)_{\mathrm{JM}-1} + (\Delta^p y)_{\mathrm{JM}-2}}, \tag{114b}$$

since $\nu_{i,1} = \nu_{i,\mathrm{JM}} = 0$.

6 Polar Filters

In the dynamical core, we apply a polar Fourier filter to the tendencies of all prognostic variables. The purpose of the polar filter is to avoid linear computational instability due to the convergence of the meridians near the poles. The filter acts poleward of about 45° latitude, and its strength is gradually increased towards the pole by increasing the number of affected zonal wavenumbers and the amount by which they are damped. The polar filter is also applied to the diagnostic ω.

Let $\psi_{i,j}$ denote a single level of any of the tendencies to be filtered. Its zonal Fourier expansion is:

$$\psi_{i,j} = \sum_{m=0}^{\mathrm{IM}/2} \hat{\psi}_{m,j} \exp(-\imath m \lambda_i),$$

where $\hat{\psi}_{m,j}$ is the complex amplitude of the mth zonal wavenumber and $\imath = \sqrt{-1}$. The filtered tendency, $\overline{\psi}_{i,j}$, is

$$\overline{\psi}_{i,j} = \sum_{m=0}^{\mathrm{IM}/2} \xi_{m,j} \psi_{m,j} \exp(-\imath m \lambda_i), \tag{115}$$

where the filter coefficients ξ are given by:

$$\xi_{m,j} = \min \left[1, \left(\frac{\cos(\phi_j)}{\cos(\phi_{\mathrm{JM}/4})} \frac{1}{\sin(m\frac{\pi}{\mathrm{IM}})} \right)^n \right]. \tag{116}$$

The rationale for the form of the filtering coefficients is the same as in Arakawa and Lamb (1977). Crudely speaking, for $n = 1$ this filtering "slows-down" the zonal propagation of each zonal component enough to satisfy the same stability criterion as is required by the shortest wave at a particular latitude—in this case 45°. Arakawa and Lamb (1977) use the meridional grid size, rather than the zonal grid size at 45° latitude, and they use the filter more selectively, treating only the gravity waves by smoothing only the mass divergence and the pressure-gradient term, rather than the entire tendencies. We found that applying it to the tendencies made the model more stable without adversely affecting the results. Also, if the filter is applied more selectively, one must be careful of how it interacts with the inertial instabilities discussed in section 5.6.4. We have also found it useful to use $n = 2$, which provides additional filtering near the pole and enhances stability.

Note that in this form the polar filter is only appropriate for grids with equal spacing in longitude. Modifying the filter for more general grids should be straightforward; for example, one can first interpolate all fields to be filtered to a uniform grid as fine as the finest spacing on the non-uniform grid and then apply the same scheme. Another possibility is to design a local filter that approximates the Fourier filter for a uniform grid. Since we have not started working with non-uniform grids, we have not tried to develop such schemes.

7 Time Differencing

As discussed in the introduction, the task of the dynamical core is limited to computing the dynamical contributions to the tendencies of all state variables. With time continuous, these depend only on the instantaneous state. For some explicit time differencing schemes, such as the leap-frog or the Euler-backward, these tendencies depend on the state at a single time level and are independent of the particular time-differencing chosen. But for multi-level explicit schemes and for all implicit schemes, the tendencies depend on the time differencing and on the size of the time step.

In the ARIES-GEOS core, the argument list contains two time levels of the state variables and the time step. This argument list can accommodate the most commonly used, explicit or implicit, time-differencing scheme. In Version 2 we support only explicit schemes. When the specified time step is less than or equal to zero, the core returns the explicit, single-level tendencies. When a positive time step is specified, the core returns "economical explicit" tendencies, using the scheme of Brown and Campana (1978), as described below. We plan to include semi-implicit differencing in future versions of the core.

7.1 The Brown-Campana Scheme

Brown and Campana (1978) proposed an explicit scheme to use in conjunction with leap-frog differencing that relaxes somewhat the instability condition for gravity waves. The scheme does not affect the advection or inertial terms. The idea is to average the pressure gradient force over three time levels. This can be accomplished very simply when using a standard leap-frog scheme by updating the mass field (potential temperatures and surface pressure in our case) first, then computing the pressure gradient at the three levels and taking an appropriate average. An even simpler strategy, which is equivalent when the pressure gradient force is linearized, is to average the three time levels of the mass field and only compute the pressure gradient once, using the averaged values. We take the latter approach, simplifying it still further by using the averaged mass field only for selected parts of the pressure gradient calculation.

We finite difference the momentum equation in time as follows:

$$\frac{\mathbf{v}^{n+1}-\mathbf{v}^{n-1}}{\Delta t} = -\nabla\Phi^* - \left(c_p\theta\frac{dP}{d\pi}\right)^n \nabla\pi^* + (\text{ all other terms })^n, \tag{117}$$

where the Φ^* are obtained from the hydrostatic equation:

$$\Phi^*_{\mathrm{LM}} = \Phi_s + c_p\overline{\theta_{\mathrm{LM}}}^t(\hat{P}_{\mathrm{LM}+1} - P_{\mathrm{LM}})^n, \tag{118}$$

$$\Phi^*_l = \Phi^*_{l+1} + c_p[(P_{l+1}-\hat{P}_{l+1})^n\overline{\theta_{l+1}}^t + (\hat{P}_{l+1}-P_l)^n\overline{\theta_l}^t], \quad \text{for } l = 1, \mathrm{LM}-1, \tag{119}$$

and

$$\pi^* = \overline{\pi}^t. \tag{120}$$

Here the $\overline{(\ \ )}^t$ denotes the three time level average

$$\overline{\pi}^t = \alpha_E(\pi^{n+1}+\pi^{n-1}) + (1-2\alpha_E)\pi^n. \tag{121}$$

As pointed out by Brown and Campana (1978), the averaging parameter, α_E, must be chosen carefully to maximize the time step. The best value depends on the strength of the Robert (1966) time filter used to control the splitting of solutions with the leap-frog. We use $\alpha_E = .2475$, which is near optimal for a time-filtering parameter of .05. We emphasize that the Robert filter is not done by the dynamical core, only the Brown-Campana smoothing of the pressure gradient that enters the momentum tendencies returned by the core.

Another point to note is that the dynamical core will compute a completely updated mass field at time level $n + 1$ only if the tendencies due to all other (non-dynamical) processes are input. However, it is not essential to do this to obtain the time step improvement, since what matters is the treatment of the gravity waves.

8 Using Subroutine DYCORE

The dynamical core is accessed by a call to FORTRAN subroutine DYCORE. Inputs to the routine include the state variables, various parameters that specify the horizontal and vertical grids, and some physical constants. The outputs of the routine are the updated time tendencies of all state variables. The state variables themselves are not modified.

In a typical GCM application would use the following procedure at each time step:

- Compute the "physics" tendencies, storing then in UOI, VOI, POI, QOI (PII would normally be zero, since sources or sinks of mass are usually ignored).
- Call DYCORE, which would add the dynamical contributions to the tendencies.
- Add the contribution of any horizontal diffusion.
- Perform the time stepping, including any time filtering that may be needed, to obtain updated values of the state variables.

8.1 The Argument List

The following is a listing of the SUBROUTINE declaration and the "banner" that is included at the top of the DYCORE source code. The banner describes the argument list and the routine's storage requirements.

```
      SUBROUTINE DYCORE ( IM,JM,JDIM,LM,SIG,PTOP,KM,DT,
     .                    OMEGA, CP, RGAS, AE,
     .                    PHS  ,PKH,
     .                    PIB  ,UOB  ,VOB  ,POB  ,QOB,
     .                    PIM  ,UOM  ,VOM  ,POM  ,QOM,
     .                    PII,  UOI,  VOI,  POI,  QOI,
     .                    OMG,  VOR,  DIAG )

C  INPUT ARGUMENT DESCRIPTION

C     IM .... Number of Grid Intervals in Zonal      Direction
C     JM .... Number of Grid Intervals in Meridional Direction
C     JDIM .. Meridional (Second) Dimension of Input  Fields
```

```
C     LM .... Number of Vertical Levels
C     SIG ... (LM+1): Sigma at Interfaces. SIG(1)=0; SIG(LM+1)=1
C     PTOP .. Model Top Pressure at Sigma = 0.0
C     KM .... Number of Scalars, Including H2O, but not Theta.
C     DT .... Time-Step fron n-1 to n+1 (Seconds)

C     OMEGA.. Rotation rate (rad/sec)
C     CP..... Specific heat at constant pressure (J/(kg K))
C     RGAS... Gas contant (J/(kg K))
C     AE..... 'Earth' radius (meters)

C     PHS ... (IM,JDIM): Surface Geopotential (m * m/sec**2)
C     PKH ... (IM,JDIM,LM+1): (P/P00)**KAPPA (Not used if PTOP=0)

C     PIB ... (IM,JDIM):    Mass (Psurf-Ptop) mb  at Current  Time-Level
C     UOB ... (IM,JDIM,LM): Zonal      Wind   m/s at Current  Time-Level
C     VOB ... (IM,JDIM,LM): Meridional Wind   m/s at Current  Time-Level
C     POB ... (IM,JDIM,LM): Potential Temp.   K   at Current  Time-Level
C     QOB ... (IM,JDIM,LM,KM): Scalar Fields      at Current  Time-Level

C     PIM ... (IM,JDIM):    Mass (Psurf-Ptop)     at Previous Time-Level
C     UOM ... (IM,JDIM,LM): Zonal      Wind       at Previous Time-Level
C     VOM ... (IM,JDIM,LM): Meridional Wind       at Previous Time-Level
C     POM ... (IM,JDIM,LM): Potential Temperature at Previous Time-Level
C     QOM ... (IM,JDIM,LM,KM): Scalar Fields      at Previous Time-Level

C  OUTPUT ARGUMENT DESCRIPTION-- Tendencies are in per second.

C     PII ... (IM,JDIM):       Updated Surface Pressure   Time-Tendency
C     UOI ... (IM,JDIM,LM):    Updated Zonal Wind         Time-Tendency
C     VOI ... (IM,JDIM,LM):    Updated Meridional Wind    Time-Tendency
C     POI ... (IM,JDIM,LM):    Updated PI-Weighted Theta  Time-Tendency
C     QOI ... (IM,JDIM,LM,KM): Updated PI-Weighted Scalar Time-Tendency

C     OMG ... (IM,JDIM,LM): Omega Diagnostic (mb/sec)
C     VOR ... (IM,JDIM,LM): Vorticity Diagnostic  (1/sec)
C     DIAG .. Logical (On/Off) Flag for Diagnostics



C  NOTES:
C      (1) JDIM is to be used for DIMENSION Purposes ONLY
C          Vectorization will be performed over IM*JM.
C      (2) The Vertical Layers are numbered from TOP(1) to BOTTOM(LM).
C      (3) All Time-Tendencies are INCREMENTED (bumped).
C          The Momentum Time-Tendencies ARE NOT mass-weighted.
C          The Potential Temperature and Scalar Time-Tendencies ARE
C          mass-weighted (by PI).
C      (4) JM is 180 degrees divided by the meridional grid size.
C      (5) UXX(I,J) are located half a grid interval EAST of PXX(I,J).
C          VXX(I,J) are located half a grid interval SOUTH of PXX(I,J).
C      (6) If PTOP>0, the PKH MUST be defined.
C      (7) The previous time level fields (PIM,UOM,etc) are used for the
C          economical explicit calculation done in conjunction with
C          leap-frog steps. If you are not doing leap-frog or do not
C          wish to have economical explicit tendencies, pass DT<=0.

C  SPACE REQUIREMENTS:
C      (1) Takes IM*JM*19+4*JM+2*IM words from the heap for STATIC storage;
C          these are kept throughout the run.
C      (2) Takes IM*JM*(LM+25) + 3*LM + 1 words from the heap for DYNAMIC
```

```
C          storage when PTOP=0; for PTOP!=0, add IM*JM*LM words.
C          All of this storage is freed before returning.
```

8.2 Comments

- The argument JDIM is provided in case the calling program has the state variables organized by level rather than variable, or has extra latitudes.
- With PTOP set to zero, the code economizes by raising only the surface pressure to the *kappa*. If PTOP is non-zero the code expects the $(\frac{p}{p_o})^\kappa$ at the interfaces to be passed in the array PKH. This is done to avoid costly recomputations of this factor, which is usually needed outside the dynamical core. If PTOP is zero, the input variable PKH is completely ignored; it need not be defined, or even allocated as an array. In this case we are not concerned about duplicating the exponentiation.
- The code sets the grid according to the values of IM and JM. This is done on the first call or whenever IM or JM change from the previous call, and the grid is saved a dynamically allocated static space. The vertical grid is inexpensive to compute and so it is reset on each call.
- In the current version the time step is used only for computing Brown-Campana tendencies. It is also used as a flag for these tendencies, which are only computed when DT is greater than zero. If DT is less than or equal to zero, the code returns an explicit tendency computed with the PIB, UOB, etc. state variables, and the PIM, UOM, etc. are ignored.

9 Results

In this section we summarize results from two studies in which this dynamical core was evaluated. The first, Takacs and Suarez (1995), compares it to and earlier version by analyzing full GCM calculations with the two codes. The second study uses the benchmark calculation for dynamical cores that was proposed by Held and Suarez (1994) to compare our dynamical core to the a version of the spectral core used at NOAA's Geophysical Fluid Dynamics Laboratory (GFDL).

9.1 Comparisons with Version 1 at Low and High Resolution

In this section, we examine the climate statistics produced by the GEOS GCM and their sensitivity to horizontal resolution and order-of-accuracy. We compare the climatology of a high res9olution "control" simulation using Version 1 of the dynamical core, with three low-resolution simulations. As mentioned in the introduction, Version 1 is very similar to Version 2, except that it uses second order differencing for the horizontal advection terms in both the momentum and thermodynamic equation. The first of the low resolution exypariments uses again uses Version 1; the second uses Version 2 as described in this report; and the third uses Version 2, adding fourth order differencing of advection in the thermodynamic and moisture equations.

All four experiments were run for a period of 26 months, of which we analyze the last two years. We have focused on the performance of model's dynamics and have performed an extensive analysis of the model's general circulation statistics, including transient and stationary variances and transports. Here we concentrate on the changes in the zonal mean flow when either horizontal resolution or order of accuracy are increased. We find that one of the most sensitive quantities is the momentum transport by transient eddies, and that accuracy of vorticity advection has a stronger effect on the zonal mean statistics than the accuracy of temperature or moisture advection.

In addition to the dynamical core, the GEOS GCM includes a full set of sub-grid parameterizations. Penetrative and shallow cumulus convection are parameterized using the Relaxed Arakawa Schubert (RAS) scheme of Moorthi and Suarez (1992), coupled with a Kessler-type scheme for the re-evaporation of falling rain (Sud and Molod, 1988). The infrared and solar radiation parameterizations follow closely those described by Harshvardhan et al. (1987). Turbulent eddy fluxes of momentum, heat and moisture in the surface layer are calculated using stability-dependent bulk formulae based on Monin-Obukhov similarity functions. Above the surface layer, turbulent fluxes of momentum, heat and moisture are calculated by the Level 2.5 Mellor-Yamada type closure scheme of Helfand and Labraga (1988), which predicts turbulent kinetic energy and determines the eddy transfer coefficients used for a bulk formulation. For a complete description of the GEOS GCM, refer to Takacs, et al. (1994).

Figure (8) shows the annual and zonal mean zonal wind for the control run at 2^o x 2.5^o resolution (8d), and differences from the control using three version at 4^o x 5^o resolution (8a through 8c). Figure (8a) depicts results from the same model version as the control, i.e., the fully second-order dynamical core. We see a very clear systematic bias in the zonal mean jet, particularly in the southern hemisphere, which is associated with an equatorward shift of the jet. Figure (8b) depicts the same difference but using fourth-order differencing in the momentum equation and second-order advection of θ and q. We see a very significant improvement in the jet structure with a decrease in the systematic error by more than 50 %, as compared with the high resolution results. Finally, figure (8c) shows the results when the advection of θ and q is also done at fourth-order accuracy. Here we see that practically all of the systematic bias in the zonal wind has been removed.

Figure 8: Simulated zonal wind from the high resolution control and differences with the three low-resolution runs. See text for details.

Given these changes in the zonal mean flow, we may anticipate significant changes in the eddy transports of heat and momentum. Figure (9) is similar to figure (8) but for the annual and zonal mean momentum flux due to transient waves, $[\overline{u'v'}]$. We clearly see in figure (9a) that the second-order GEOS GCM run at low resolution produces a strong equatorward shift of the momentum transport, with errors comparable in magnitude to the total flux itself. These errors again are substantially reduced by using fourth-order vorticity advection, and virtually eliminated with the addition of fourth-order advection of θ and q.

Figures (10) and (11) show the sensitivity to resolution and order of accuracy for the heat and moisture transports.

Figure 9: Same as previous figure, but for transient eddy momentum transport.

Figure 10: Same as previous figure, but for transient eddy heat transport.

Figure 11: Same as previous figure, but for transient eddy moisture transport.

9.2 Results of the Idealized Forcing Test and Comparison with a Spectral Code

In this section we present detailed results from the Held and Suarez (1994) benchmark calculation for the intercomparison of dynamical core. In this calculation the model is forced with a simple Newtonian heation and damped by Rayleigh friction and run over a smooth lower boundary. The objective is to evaluate the performance of the dynamics independently of the physics. In full GCM comparisons, such as the ongoing AMIP program, the models differ in mane complicated ways, which makes the assesment of individual portions, such as the dynamics, very difficult. The reader is refered to Held and Suarez (1994) for a discussion of intercomparison issues and for details on how the calculation is performed.

Here we present the results of this benchmark for the Aries/GEOS dynamical core and compare them with similar results produced by Isaac Held at the Geophysical Fluid Dyanmics Laboratory in Princeton using a spectral dynamical core. Further details on the spectral calculation are also given in Held and Suarez (1994).

The models were run for 1200 days at four different resolutions. All results presented are averages over the last 1000 days, after the solutions have equilibrated. The resolutions used for the spectral model are T21, T30, T42, and T63, where the numeral refers to the maximum number of zonal waves present. The resolutions used for the grid point model are 6° latitude x 7.5° longitude, 4° x 5°, 3° x 3.75°, and 2° x 2.5°. For convenience, we denote these models as G24, G36, G48, and G72, where the numeral refers to half of the number of gridpoints around a latitude circle.

The first two sets of figures show zonally averaged quantities as a function of latitude and sigma. The first set shows the mean fields and the second set quadratics of eddy quantities. A third set shows the vertically interagrated zonal spectrum of selected quadratics. The last set summarizes the resolution dependence of several important quantities by comparing line plots of zonal mean values.

ZONAL MEAN FIELDS

QUADRATIC QUANTITIES

ZONAL SPECTRA

VERTICAL MEANS

10 Final Remarks

We have presented a detailed description of the Eulerian grid-point dynamics currently being used as the "dynamical core" of global atmospheric modeling at Goddard. This dynamical core is written in a modular form that allows easy implementation, assuming the GCM's variables are already stored on an Arakawa C grid. In addition to a detail discussion of the numerics, including the introduction of a new fourth-order scheme, we have described the usage of the routine and presented results from two evaluations of the core.

All of these results, as well as the Fortran source code are being made available over the network. To obtain access to these or for further information send e-mail to suarez@climate.gsfc.nasa.gov or to w3llt@dao.gsfc.nasa.gov.

References

Arakawa, A., 1966: Computational design for long-term numerical integration of the equations of fluid motion: Two-dimensional incompressible flow. Part I. *J. Comput. Phys.*, **1**, 119-143.

Arakawa, A., 1972: Design of the UCLA general circulation model. *Tech. Report No.7, Dept. Meteor., UCLA*, Los Angeles CA 90024. *Mon. Wea. Rev.*, **109**, 18-36.

Arakawa, A. and V.R. Lamb, 1977: Computational design of the basic dynamical processes of the UCLA general circulation model. in *Methods in Computational Physics*, J Chang ed., Academic Press, **17**, 173-265.

Arakawa, A. and V.R. Lamb, 1981: A potential enstrophy and energy conserving scheme for the shallow water equations. *Mon. Wea. Rev.*, **109**, 18-36.

Arakawa, A. and M.J. Suarez, 1983: Vertical differencing of the primitive equations in sigma coordinates. *Mon. Wea. Rev.*, **111**, 34-45.

Brown, J.A. and K. Campana, 1978: An economical time-differencing system for numerical weather prediction., *Mon. Wea. Rev*, **106**, 1125-1136.

Burridge, D.M. and J. Haseler, 1977: A model for medium range weather forecasting—adiabatic formulation, *Tech. Report. No. 4, European Center for Medium Range Weather Forecasts*, Brachnell, Berkshire, UK.

Harshvardhan, R. Davies, D. A. Randall, and T. G. Corsetti, 1987: A fast radiation parameterization for atmospheric circulation models. *J. Geophys. Res.*, **92**, 1009-1016.

Held, I.M. AND M.J. Suarez, 1994: A proposal for the intercomparison of the dynamical cores of atmospheric general circulation models. Submitted to *Bull. Am. Met. Soc.*

Helfand, H. M., and J. C. Labraga, 1988: Design of a non-singular level 2.5 second-order closure model for the prediction of atmospheric turbulence. *J. Atmos. Sci.*, **45**, 113-132.

Hollingsworth, A., P. Kållberg, V. Renner, and D.M. Burridge, 1983: An internal symmetric computational instability, *Quart. J. R. Met Soc.* , **109**, 417-428.

Kalnay, E., M. Kanamitsu, J. Pfaendtner, J. Sela, M. Suarez, J. Stackpole, J. Tuccillo, L. Umscheid, and D. Williamson, 1989: Rules for the interchange of physical parameterizations, *Bull. Am Met. Soc.*, **70**, 620-622.

Moorthi, S., and M. J. Suarez, 1992: Relaxed Arakawa Schubert: A parameterization of moist convection for general circulation models. *Mon. Wea. Rev.*, **120**, 978-1002.

Phillips, N.A., 1974: Application of Arakawa's energy conserving layer model to operational numerical weather prediction. *Office Note 104, National meteorological Cen-*

ter, NWS/NOAA 40pp.

Robert , N.A., 1966: The integration of a low-order spectral form of the primitive meteorological; equations. *J. Meteor. Soc. Japan*, **44**, 237-245.

Sadourney, R., 1975: The dynamics of finite difference models of the shallow water equations, *J. Atmos. Sci.*, **32**, 680-689.

Sud, Y. C., and A. Molod, 1988: The roles of dry convection, cloud-radiation feedback processes and the influence of recent improvements in the parameterization of convection in the GLA GCM. *Mon. Wea. Rev.*, **116**, 2366-2387.

Takacs, L.L. and M.J. Suarez, 1995: On the impact of horizontal resolution and order of accuracy on the climate statistics of the GEOS GCM. In preparation.

Takacs, L. L. , A. Molod, and T. Wang, 1994: Goddard Earth Observing System (GEOS) General Circulation Model (GCM) Version 1, [Documentation available from L. Takacs, NASA/GSFC, Code 910.3, Greenbelt, MD 20771 (w3llt@almagest.gsfc.nasa.gov)].

Takano, K. and M.G. Wurtele, 1982: A fourth-order energy and potential enstrophy conserving difference scheme, Air Force Geophysics Laboratory Report AFGL-TR-82-0205, (NTIS AD-A126626), AFGL Hanscom AFB, Massachustts, 01731, 85pp.